Measurements of the lead-hydrocarbon cross section ratio for charged-current neutrino interactions

A thesis submitted in partial fulfillment of the requirement for the degree of Bachelor of Science in Physics from The College of William and Mary

by

William Frederick Bergan

Accepted for HONORS
(Honors or no-Honors)

Jeffrey Nelson, Director

Gina L. Hoatson
Gina Hoatson, Physics

Patricia L Vahle
Patricia Vahle, Physics

Nahum Zobin, Mathematics

Williamsburg, VA
April 28, 2015

Measurements of the lead-hydrocarbon cross section ratio for charged-current neutrino interactions

William Bergan

May 11, 2015

Abstract

Studying the neutrino cross sections of various materials is of great importance in the analysis of data from neutrino oscillation experiments, as well as interesting in its own right. We have examined the charged-current muon neutrino cross section ratio between lead and scintillator, with our lead target being in the MINERvA electromagnetic calorimeter. This choice has allowed us to obtain usable efficiencies out to much larger muon angles than was feasible from the upstream targets. Comparing the cross section ratio in the data and Monte Carlo, we have found that the ratios agree reasonably well as a function of neutrino energy, but with a distinct excess at low energies. However, there are significant differences between data and Monte Carlo at low and high values of Bjorken x.

I. Introduction

Neutrinos are standard-model fermions which only interact via the weak force. Due to this, they interact very rarely, making them notoriously difficult to study. There are three neutrino flavors, corresponding to the three charged leptons. Neutrino oscillation has been observed by a number of experiments, wherein neutrinos of different flavors may turn into one another as they travel, and the study of this is a promising avenue for the discovery of new physics. In order to properly interpret the results of such experiments, it is useful to know the cross sections of neutrino interactions. Besides their use in oscillation experiments, neutrino cross sections are interesting in their own right, since the cross section change depending on whether or not a nucleon is bound in a nucleus. This is due in part to the fact that the bound nucleon will have some Fermi motion within the nucleus and some binding energy. Moreover, there are theories that the nucleons themselves are modified when put inside a nucleus. This change in cross section for a bound nucleon will then give information about nuclear structure functions. For instance, a 2014 analysis by Brian Tice showed that ratio of a material's neutrino cross section to that in scintillator increased as a function of Bjorken x (the fraction of the nucleon's momentum carried by the struck quark) more quickly in larger nuclei, a phenomenon not reproduced by the simulations.[1] We will attempt to study this phenomenon further using different targets. In this analysis, we reconstructed our events using the resurrection version of the MINERvA software. We modeled the physics in the detector using the Monte Carlo (simulations made with the Monte Carlo method.) This used GENIE to model the neutrino interaction, data-constrained FLUKA to model the flux, and GEANT4 to model particle transport.[1]

There are two types of neutrino interactions: neutral current interactions, where the neutrino remains a neutrino, and charged-current interactions, where the neutrino becomes a charged lepton of the same flavor. This work will only deal with the latter. Since we are looking at muon neutrinos, we will only use events with a final state muon. Charged-current interactions may be further subdivided into different processes based on the details of the interaction. Quasielastic events involve the neutrino scattering off the nucleon as a whole. Resonance events involve the creation of a short-lived resonance, which subsequently decays. Deep inelastic scattering (DIS) events involve the neutrino interacting with a single quark inside the nucleus.

In order to compute a neutrino cross section, one would measure the total number of interactions, divide by the incident neutrino flux, and divide by the number of nucleons which may serve as scattering centers in the fiducial volume. However, we must also subtract off any backgrounds and scale our result up by the inverse of the efficiency, as well as correct for migration due to finite detector resolution. In principle, then, our neutrino cross section may be written as

$$\sigma = \frac{U(N_{events} - N_{background})}{\epsilon \Phi N_{nucleons}}$$

where ϵ is efficiency, Φ is the incident neutrino flux, $N_{nucleon}$ is the number of nucleons the fiducial region, $N_{background}$ and N_{events} are the background and observed event rates in reconstructed variables, and U is an unfolding matrix to map distributions in reconstructed variables to distributions in true variables. However, there is one additional issue: the incident flux is not well-known and introduces large errors into our computation. For this reason, we will look only at the ratios of the cross sections between two materials, so that the contribution from the flux largely cancels.

MINERvA is a neutrino cross section experiment at Fermilab and is the first experiment measuring neutrino cross sections on different materials using the same beam in the few-GeV energy range. It is located in the NuMI (Neutrinos at the Main Injector) beam, which provides the source of neutrinos for the experiment. The beam is produced by firing a stream of protons at a fixed target. This will produce a secondary beam of pions and kaons. A magnetic horn focuses particles of specific signs (positive for our study) and energies. These then decay, usually into positive muons and muon neutrinos in our case. The muons are stopped by rock, while the neutrinos are able to pass through to the MINERvA detector.

The detector itself consists, going from the upstream to the downstream end, of a series of passive nuclear targets, a tracker region consisting of scintillator, an electromagnetic calorimeter (ECAL) consisting of lead and scintillator, and a hadronic calorimeter (HCAL) consisting of steel and scintillator. Behind MINERvA is the MINOS near detector, which is able to measure the momentum of the final state muon based on its curvature in a magentic field or its stopping range. See FIG. 1. We therefore require that our muons enter the MINOS detector, which places geometrical acceptance and momentum limits on our events.

Previous analyses have studied neutrino interactions in the upstream targets and compared them with those in the tracker. We will instead look at neutrino interactions in the downstream region of the tracker and upstream part of the ECAL. Since our events will occur closer to MINOS, we will be able to accept muons traveling at larger angles relative to the beamline, giving us a larger geometric acceptance.

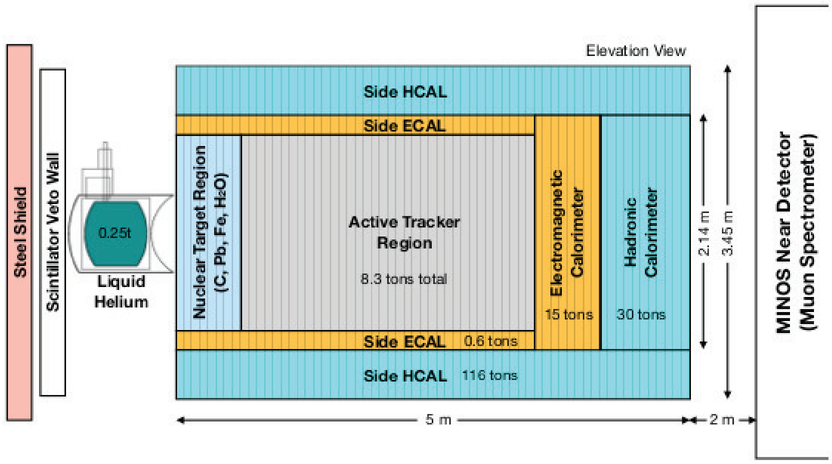

FIG. 1. The MINERvA detector.[1]

II. Methods and Results

II..1 Defining the Fiducial Volume

We first set out to determine the ideal size of the fiducial volume for the tracker and ECAL regions. In order to prevent events from the side detectors from entering our sample, we required that our events be within a hexagon with 85 cm apothem, as was done in previous analyses.[1] In order to ensure that the region in which a particular interaction happened is well-known, we defined a buffer zone around the border between the tracker and the ECAL. To determine the size of this buffer zone, we plotted the number of events in the modules near the tracker-ECAL border in data and Monte Carlo. There is a transition region of 3-4 modules during which there are some intermediate number of events, indicating that the reconstruction resolution is poor enough to contain a mix of events from the two regions, but the distribution flattens out after that. The results are plotted in FIG. 2 for the full sample, FIG. 3 for the DIS subsample,* and FIG. 4 for the quasielastic-enhanced sample.† We also looked in the Monte Carlo to plot the number of charged-current events as a function of the true and reconstructed vertex module, as can be seen in FIG. 5. This shows us that the vertices are usually reconstructed within two modules of the true one, so that we will have a relatively clean sample so long as we stay at least one or two modules away from the tracker-ECAL border. We decided on a border of 1 module in the

*The DIS subsample consists of events with invariant recoil mass $W > 2$ GeV and the momentnum transfer squared $Q^2 > 1$ GeV^2.

†The quasi-elastic enhanced subsample is defined with $W < 1.2$ GeV.

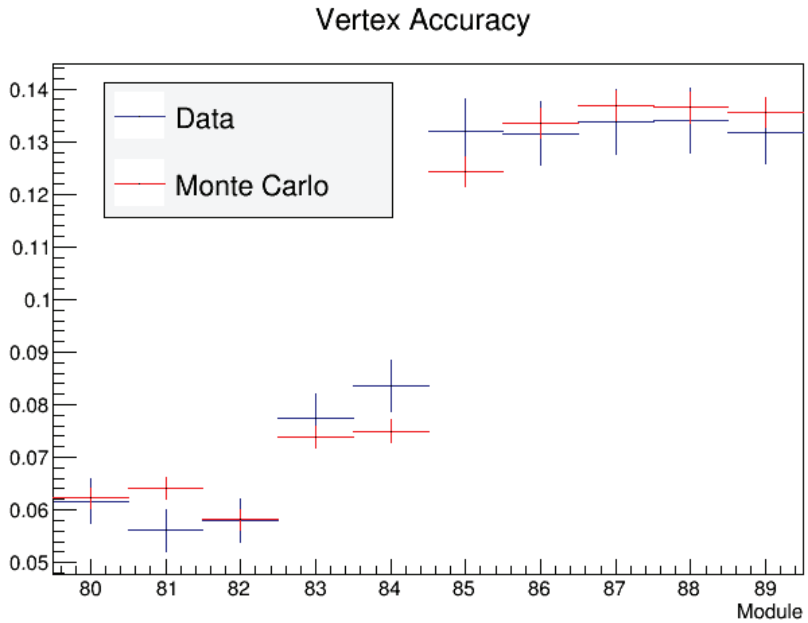

FIG. 2. The fraction of events in each module for CC inclusive events. There is good agreement between the data and Monte Carlo. Due to vertex reconstruction errors, we do not use events in the last two tracker modules and first ECAL module.

upstream part of the ECAL (2 for the DIS sample) and 2 modules in the downstream part of the tracker.

The back end of the ECAL fiducial volume is determined by the distance to the HCAL; since that part of the detector has a considerably greater amount of inert material than does the ECAL, we would like as much of our energy as possible to stay in the ECAL to retain good energy resolution. To do this, we used the data from the test beam detector[‡] to see how much energy electrons deposited at or before a given plane[§] of the test beam ECAL. This plot may be seen as FIG. 6. From this, we decided that only the first 4 modules of the ECAL (counting the buffer region) would give us sufficient electron containment, since we would still contain 80% as much energy as if we were using the full ECAL.

To determine how far upstream in the tracker we are able to go, we made efficiency[¶] histograms

[‡]The test beam detector is a scaled down version of the main detector used to study its response to different particles.

[§]There are two planes per module.

[¶]We used a different definition for the efficiency than was used later on, in that we only require the events to pass the cuts in truth, not in the reconstructed variables too.

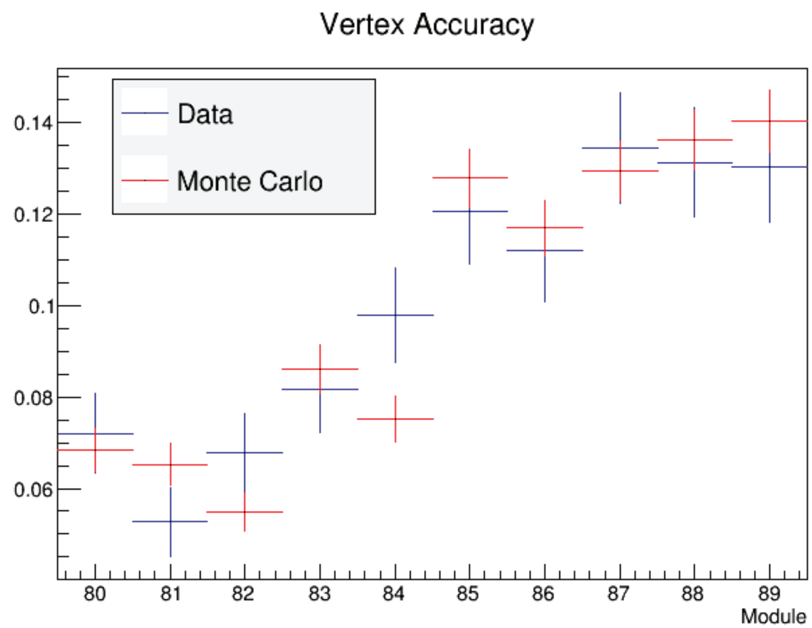

FIG. 3. The fraction of events in each module for DIS events. There is good agreement between the data and Monte Carlo. Due to vertex reconstruction errors, we do not use events in the last two tracker modules and first two ECAL modules.

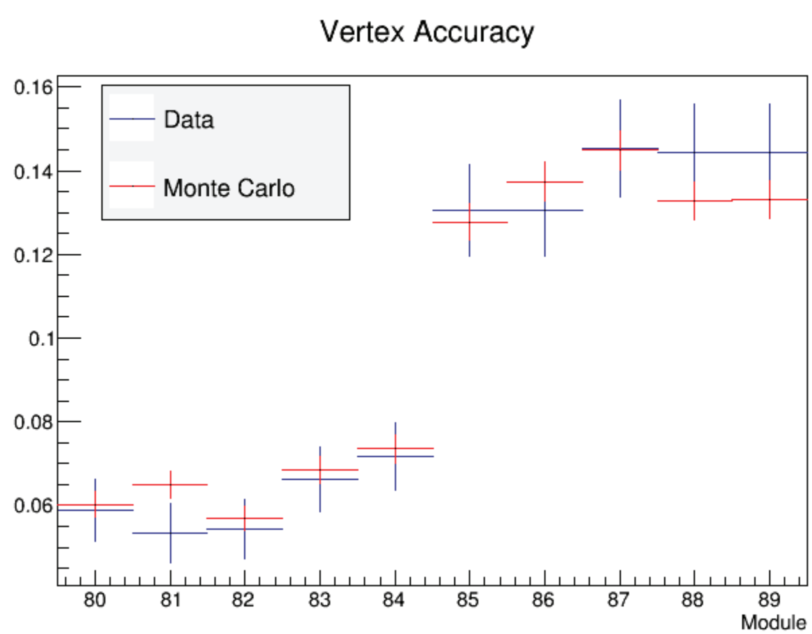

FIG. 4. The fraction of events in each module for quasielastic-enhanced events. The errors are statistical. The Monte Carlo may be a bit oversmeared. Due to vertex reconstruction errors, we do not use events in the last two tracker modules and first ECAL module.

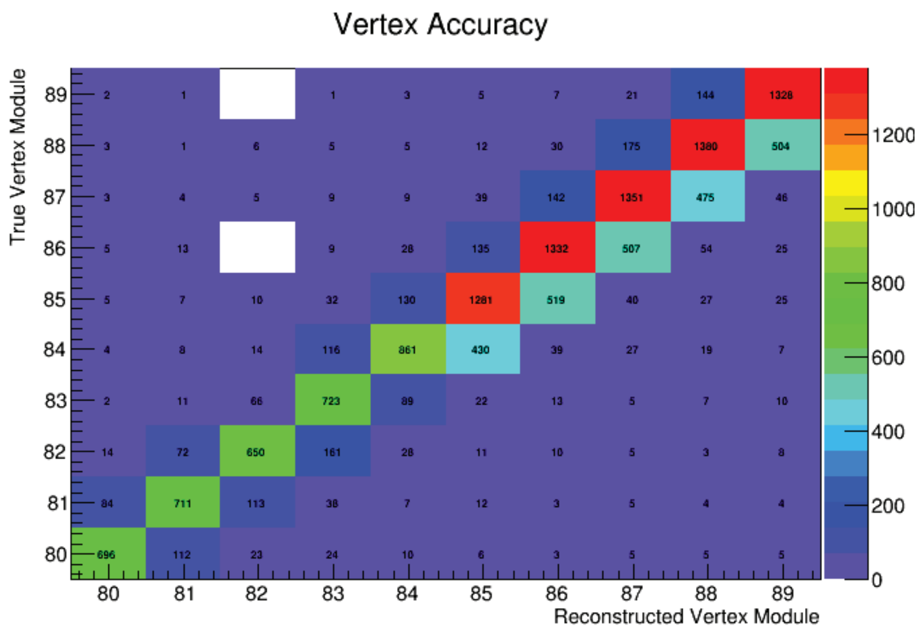

FIG. 5. The number of events for a given true and reconstructed vertex module in the Monte Carlo. We see that the vertex is correctly reconstructed within a module or two of the true vertex, and that outside such a buffer, our sample will be relatively pure.

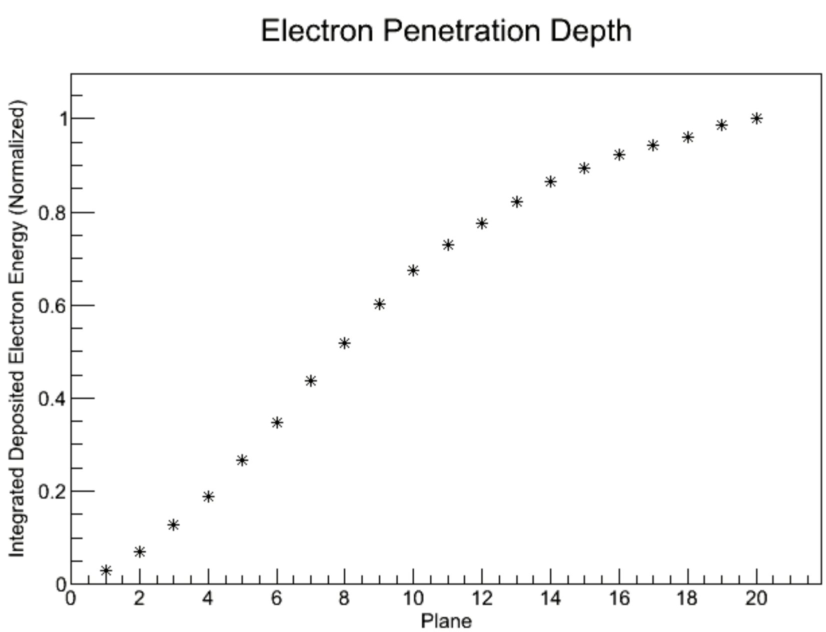

FIG. 6. The fraction of electron energy deposited at or before a given plane in the test beam ECAL data, relative to the toral energy deposited in the ECAL. Based on this plot, we ought to use only the first 4 modules (8 planes) to get a good containment of the energy.

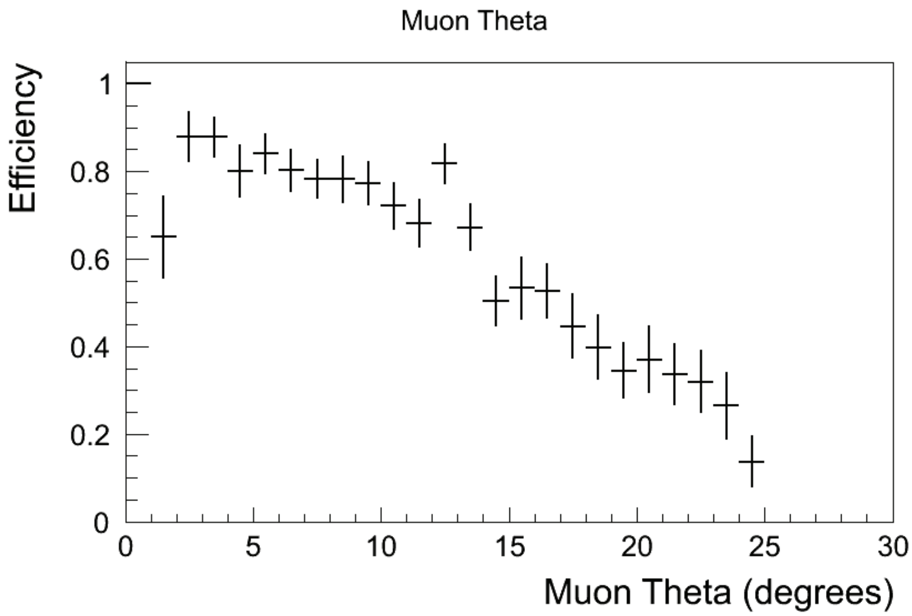

FIG. 7. The efficiency for events in tracker modules 73-82 as a function of true muon angle with respect to the beam. This is taken from the Monte Carlo with statistical and systematic errors.

in simulated data with our fiducial volume set as progressively upstream groups of ten modules. These may be seen as FIG. 7 - 9. Ultimately, we settled on using the twenty most downstream tracker modules upstream of the two modules at the tracker-ECAL boundary. Modules further upstream introduced a significant drop in efficiency and would not have given us a significant improvement in the cross section ratio statistical errors. In summary, our fiducial extends from modules 63-82 in the tracker and modules 86-88 in the ECAL.

II..2 Efficiencies

We wished to ensure that this new sample would enable us to obtain an increased angular acceptance when compared with the upstream targets analysis. To do this, we computed the efficiency as the number of charged-current muon neutrino interactions in our fiducial volume with neutrino energy between 2 and 20 GeV and no unresponsive channels in the muon's projected upstream path in the Monte Carlo that are reconstructed as such, divided by the total number of such events. In particular, this requires that the muon associated with the interaction hits the MINOS near detector, which places a natural limit on its angle and momentum. Plots of this efficiency as a function of muon angle may be seen as FIG. 10 and FIG. 11. We compared

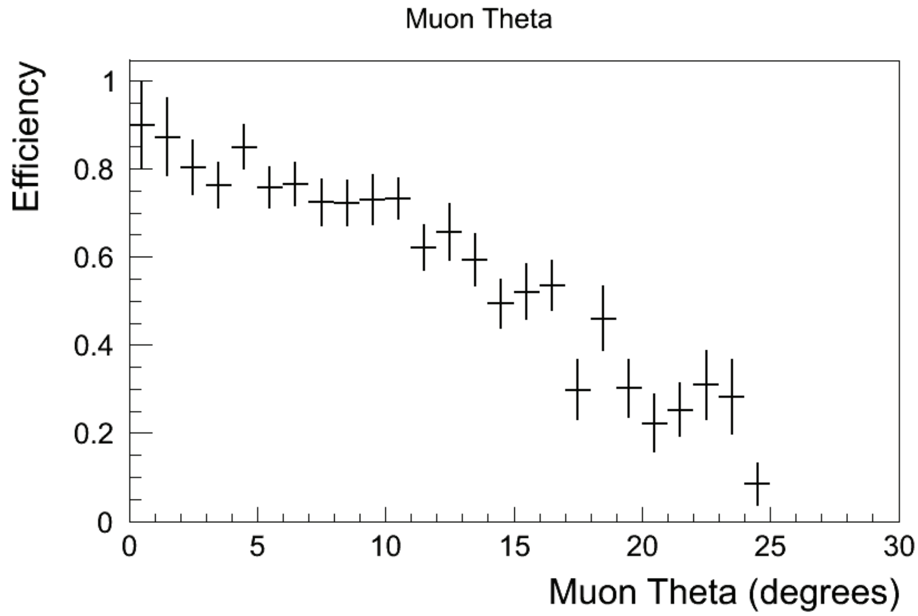

FIG. 8. The efficiency for events in tracker modules 63-72 as a function of true muon angle with respect to the beam. This is taken from the Monte Carlo with statistical and systematic errors.

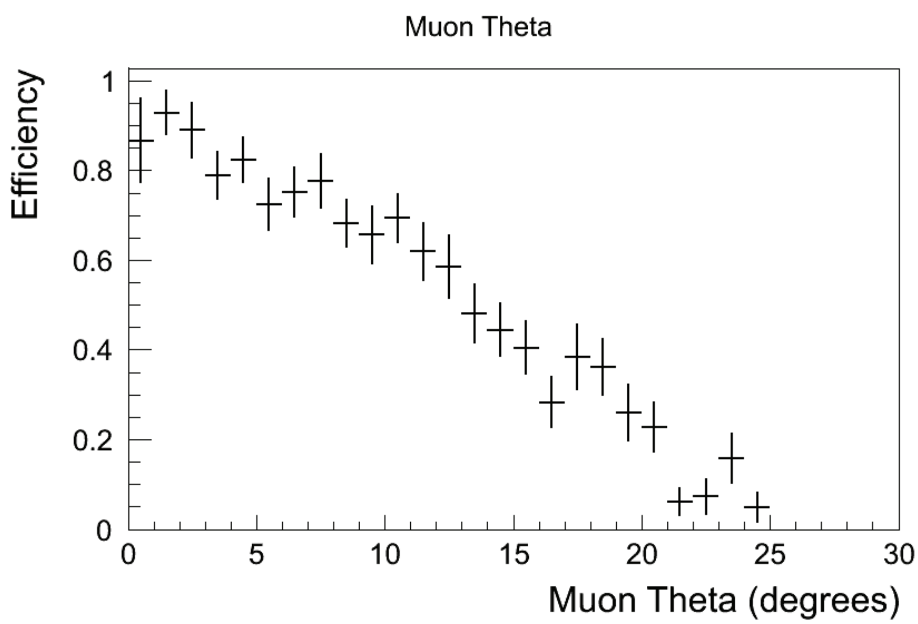

FIG. 9. The efficiency for events in tracker modules 53-62 as a function of true muon angle with respect to the beam. This is taken from the Monte Carlo with statistical and systematic errors. Note the drop at around 20 degrees relative to FIG. 7 and 8.

these values with those found by a prior analysis[1] in the upstream passive targets and at the back of the tracker in FIG. 12 and FIG. 13. We note that our efficiency in the tracker is significantly greater due to the use of a thicker fiducial volume, so that fewer events leave our sample due to a misreconstruction of the vertex. Note also that our acceptances are significantly greater than his acceptances from the upstream targets, especially at large muon angles. This will allow us to include a greater fraction of events, with muon angles up to 25°, rather than 17°. A total of 53% of the events are above 17°, but only 35% are above 25°.

Based on these results and to compare our results to those in the previous analysis[1], we defined our sample as those events which are muon charged-current interactions, with the original neutrino energy between 2 and 20 GeV and the muon travelling at an angle of no more than 25° with respect to the z-axis of the detector. Additionally, we require that there not be any dead detector elements in the upstream projected path of the muon, since that raises the possibility that the interaction had occurred further upstream than we had reconstructed. We also require that the muon be reconstructed as having a negative charge in MINOS. Finally, we require that the events be within our fiducial volume, defined in either the ECAL or tracker, as the case may be. This includes not just the module cuts described previously, but also that the interaction happen within a hexagon of apothem 85 cm, to avoid the possiblity of contamination from interactions in the side ECAL or side HCAL.

Defining our efficiency as the number of observed events in our Monte Carlo sample divided by the total number of events which are in it in truth, we find the efficiencies in our tracker and ECAL volumes. See, for example, FIG. 14 and 15. The reason for the discrepency at high energy is that the ECAL fiducial volume is much thinner than the tracker volume, so that a greater fraction of the ECAL events are reconstructed outside the fiducial volume. The corresponding plot from the Tice analysis is shown in FIF. 16. Additional efficiency plots as functions of Bjorken x, muon energy, nuclear recoil energy, and inelasticity[‖] may be seen in the Appendix.

[‖] The fraction of the neutrino's energy which goes into the nuclear recoil system.

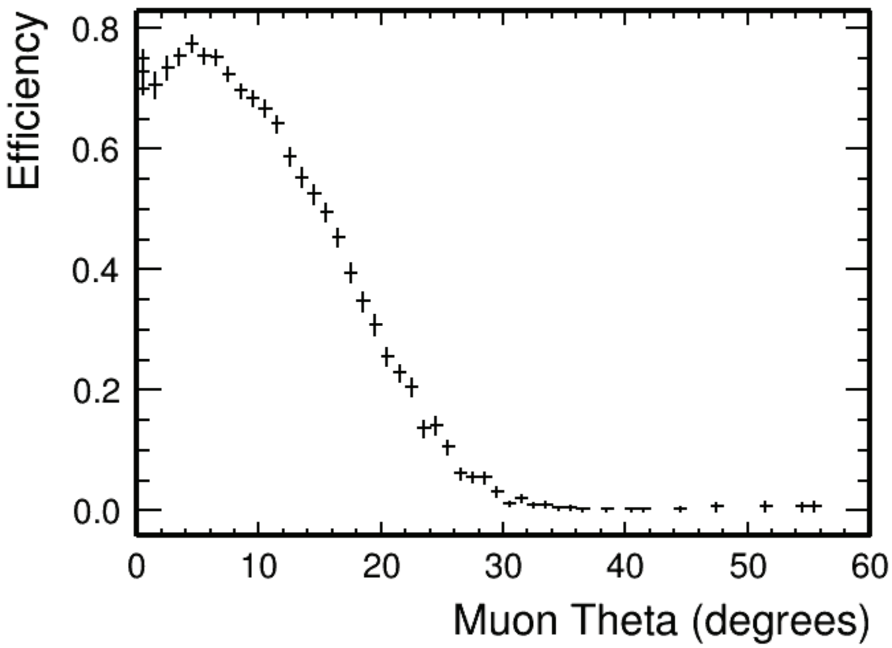

FIG. 10. Efficiency in the tracker fiducial volume as a function of true muon angle. This is taken from the Monte Carlo with statistical and systematic errors.

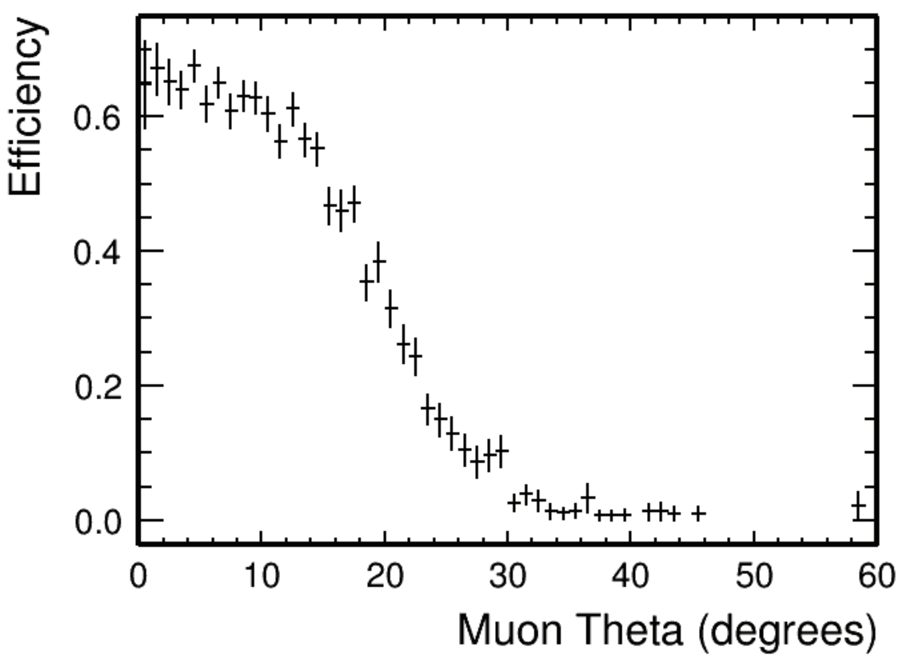

FIG. 11. Efficiency in the ECAL fiducial volume as a function of true muon angle. This is taken from the Monte Carlo with statistical and systematic errors.

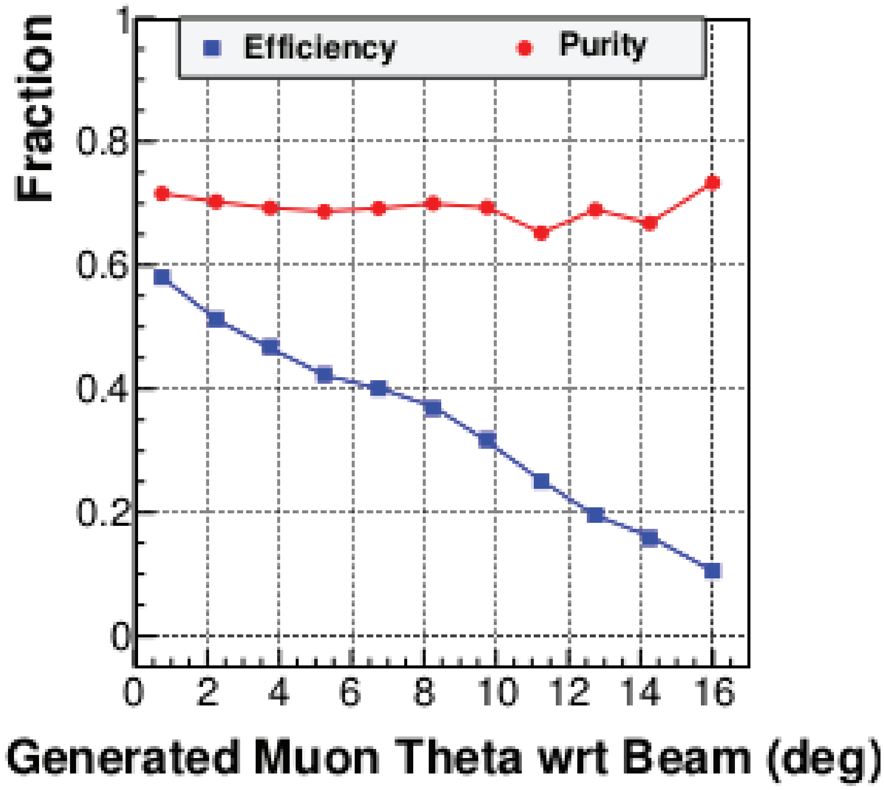

FIG. 12. Acceptance for events in the upstream target number 5.[1]

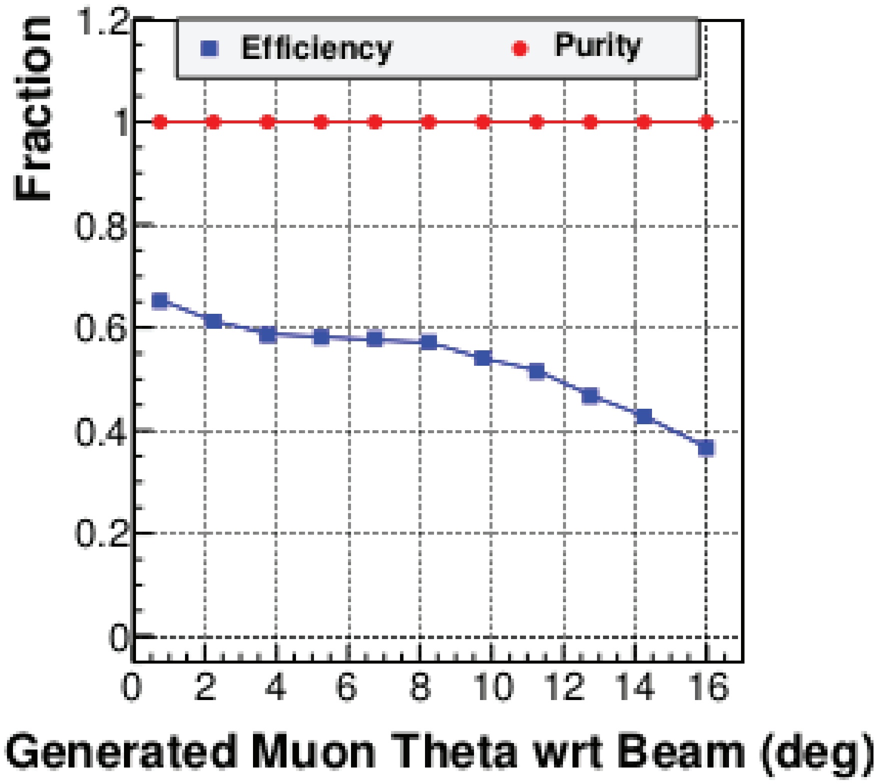

FIG. 13. Acceptance for events in the tracker, modules 75-80.[1]

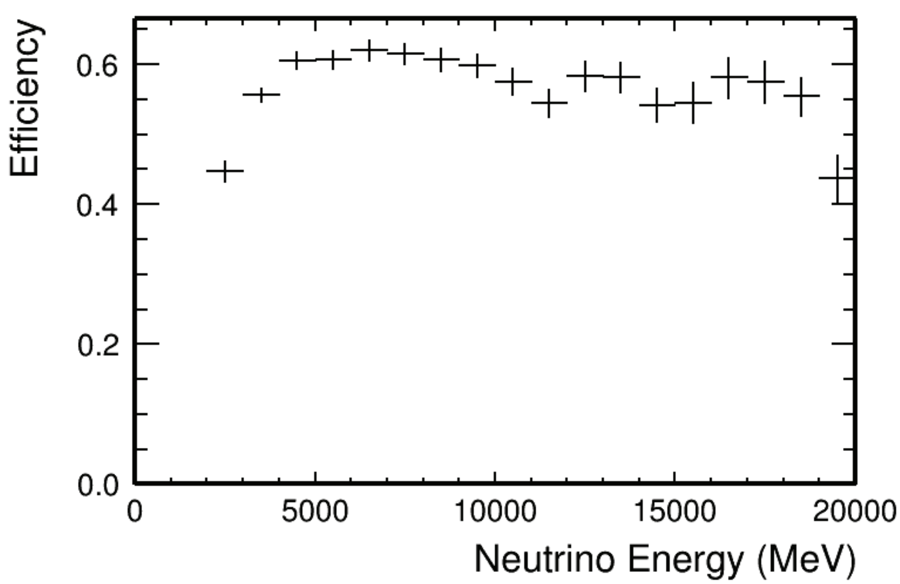

FIG. 14. Efficiency as a function of true neutrino energy in the tracker. This is taken from the Monte Carlo with statistical and systematic errors.

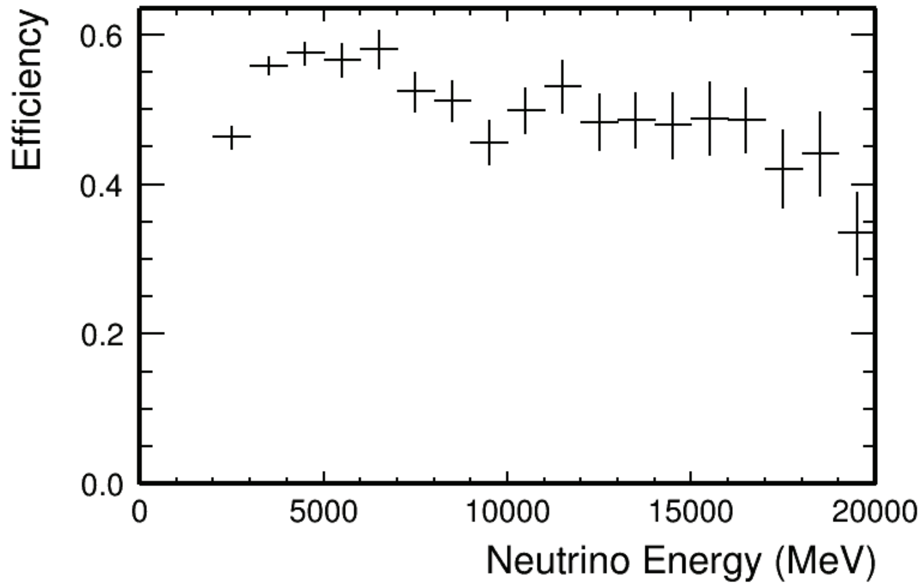

FIG. 15. Efficiency as a function of true neutrino energy in the ECAL. This is taken from the Monte Carlo with statistical and systematic errors.

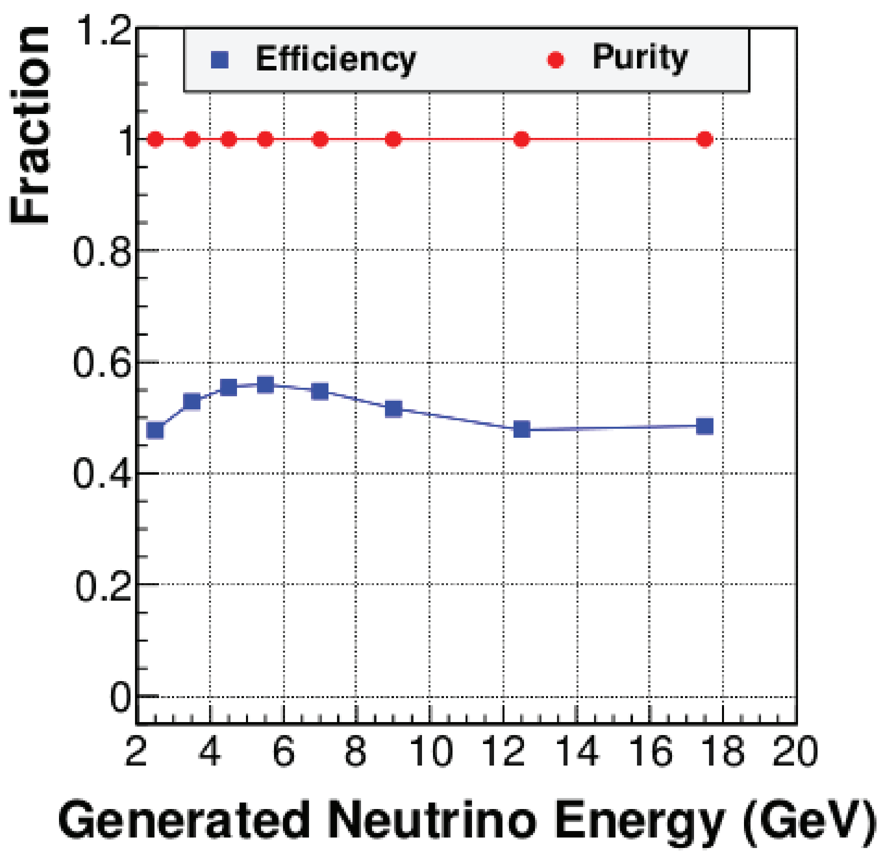

FIG. 16. Efficiency as a function of true neutrino energy in the back of the tracker, modules 75-80, as found by Brian Tice.[1]

II..3 Backgrounds

Our data contain backgrounds from various sources. We have broadly defined backgrounds as anything that is incorrectly reconstructed to be in our sample. This includes the physics backgrounds, which are events besides muon neutrino charged-current scatters, as well as backgrounds which involve a real physics event which does not fit within our desired energy, muon angle, or fiducial volume cuts. To compare with data, we scaled up the background estimate from the Monte Carlo by the number of events reconstructed in the data divided by the number of events reconstructed in the Monte Carlo. This scaling factor was 1.67 in the tracker and 1.57 in the ECAL.** A plot of the background distribution is shown in FIG. 17 for tracker backgrounds and FIG. 18 for ECAL backgrounds. The reason for the much higher backgrounds in the ECAL is due to the thinner size of the fiducial volume there, so that a larger fraction of the events are from outside the fiducial volume. Background distributions as functions of Bjorken x, muon angle, muon energy, nuclear recoil energy, and inelasticity are shown in the Appendix.

II..4 Unfolding

During reconstruction, the data measured for a particular event does not exactly match the true value, and it may result in that event being reconstructed in a different bin of the histogram. To correct for this, we use Bayesian iterative unfolding. We first make a row-normalized 2 dimensional histogram of Monte Carlo events, with the true value of the relevant variable on one axis and the reconstructed value on the other. Using these migration matrices (see FIG. 19 and FIG. 20) and our data distribution, iterative algorithms, such as RooUnfold,[8] exist to work backwards and recover an estimate of the underlying data distribution. The use of more iterations will introduce additional statistical errors. To keep errors small, we used one iteration.†† This procedure is necessary so that our reported cross sections are functions of real values, not reconstructed ones, allowing for easier interpretation of the results.

**The number of protons on target to produce the neutrino beam (POT) for the data sample was 9.44×10^{19}, while the POT for the Monte Carlo sample was 1.91×10^{20}.

††Joel Mousseau found that this was the correct choice in the upstream targets.[11]

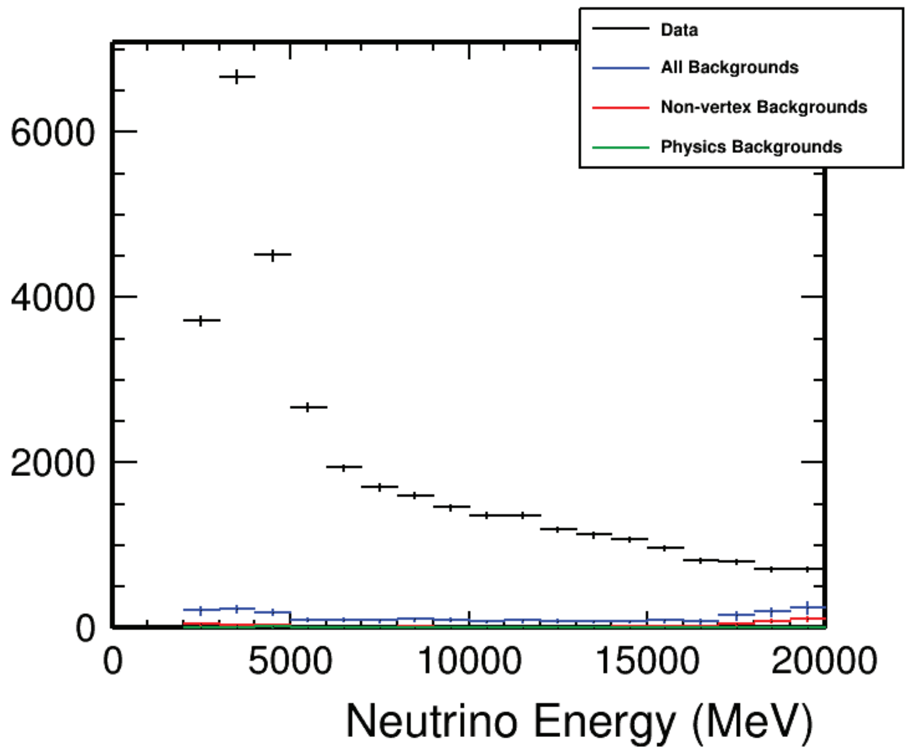

FIG. 17. Backgrounds estimated from the Monte Carlo superimposed on the data distribution in the tracker as functions of reconstructed neutrino energy. The background has statistical and systematic errors, while the data has just statistical errors. Note that the successively background curves ar cumulative.

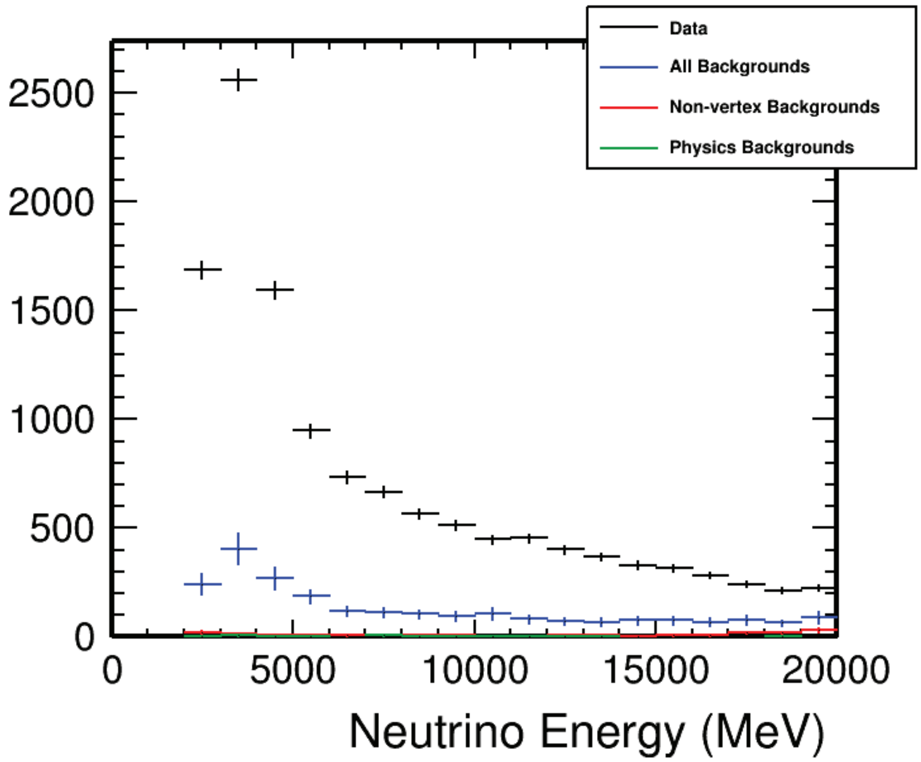

FIG. 18. Backgrounds estimated from the Monte Carlo superimposed on the data distribution in the ECAL as functions of reconstructed neutrino energy. The background has statistical and systematic errors, while the data has just statistical errors. Note that the successively background curves ar cumulative.

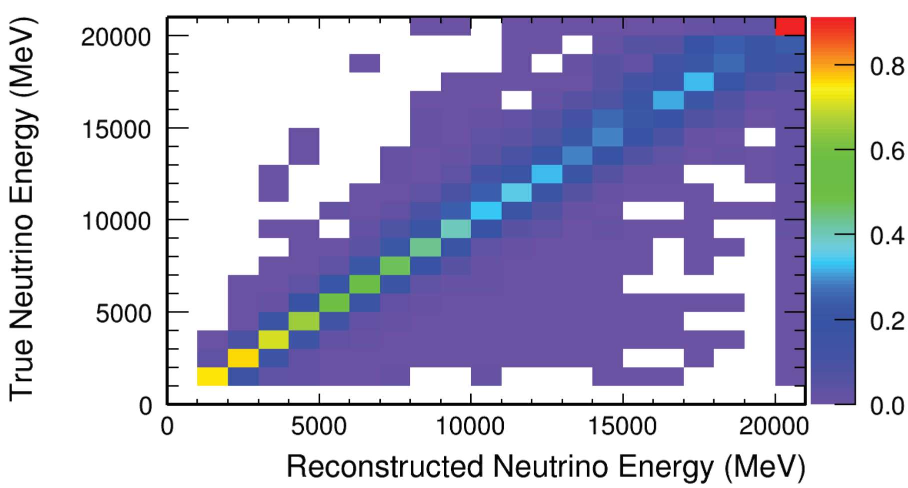

FIG. 19. Migration matrix in the neutrino energy. Note that most of the events fall on or near the diagonal, indicating good energy resolution.

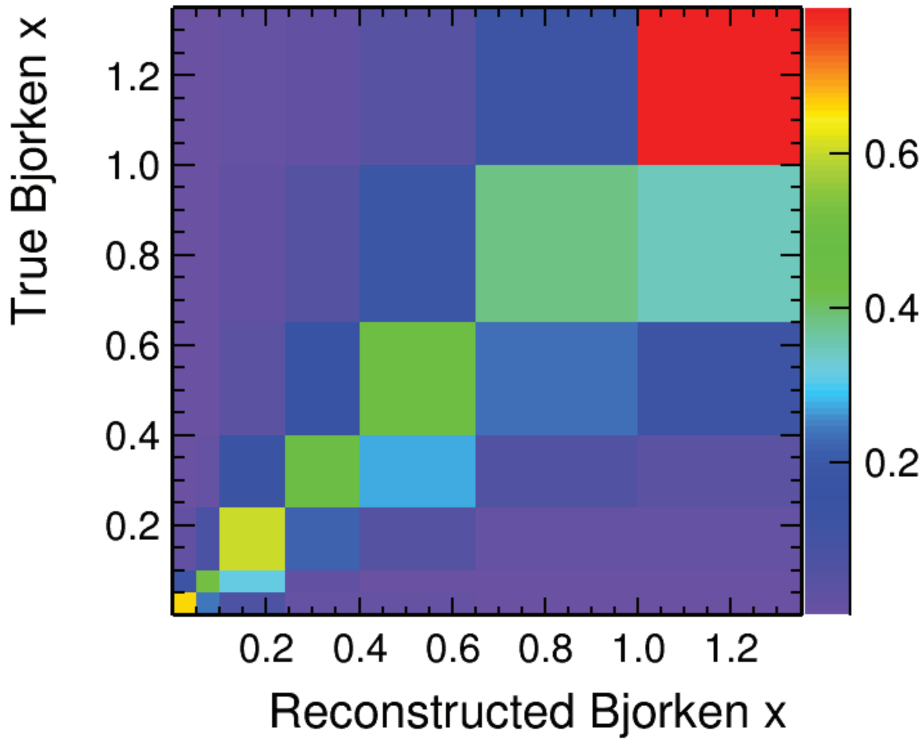

FIG. 20. Migration matrix in Bjorken x. This is also relatively diagonal, although it breaks down at high values of Bjorken x.

II..5 Scattering Center Normalization

Since different nuclei will have different numbers of nucleons for neutrinos to interact with, we wished to normalize our results relative to the number of scattering centers in our samples. To get the number of scattering centers in a plane of scintillator, we took the number from page 24 of Brian Tice's thesis[1] of 3.05×10^{28} nucleons per plane. With 40 planes in our tracker sample (20 modules, with 2 planes per module), this gives us 1.22×10^{30} nucleons. The fiducial area per plane quoted in his thesis corresponds to defining the fiducial volume as a hexagon with an apothem of 85 cm. We therefore used this as the apothem for the fiducial region of our lead planes in the ECAL, obtaining an area of 2.50 m^2. The depth of the lead planes is 2 mm $\pm$ 0.02 mm,[10] giving us a total volume of 0.005 m^3 for each plane. There are six such planes in our ECAL sample, giving us 0.03 m^3 total lead volume. Multiplying by the density of lead gives us 341 kg of lead. Dividing by the proton mass gives us 2.05×10^{29} scattering centers in the ECAL lead. However, there will be an additional 6 planes of scintillator. Using the methods described above to find the number of tracker scattering centers, we get an additional 1.83×10^{29} scattering centers, for a total

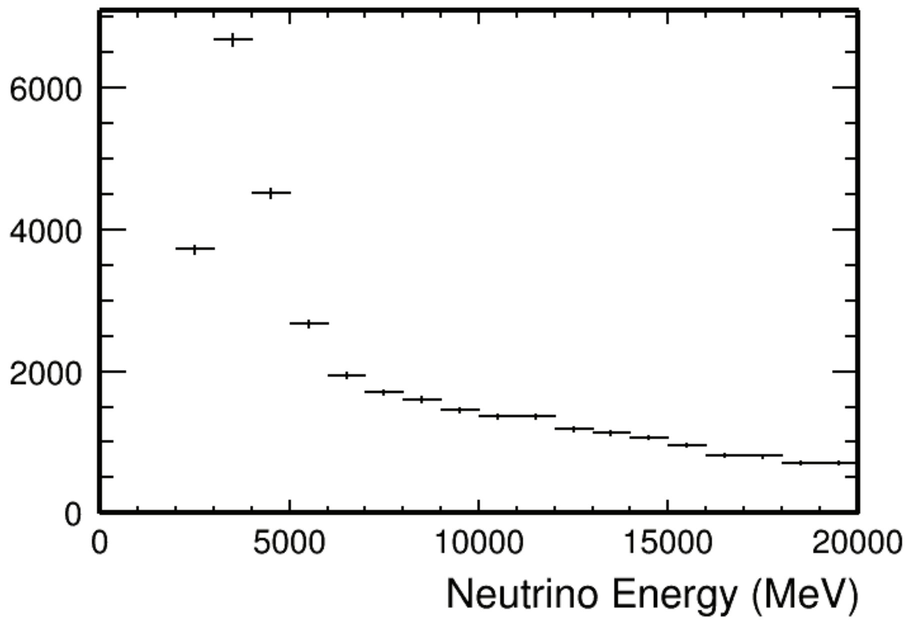

FIG. 21. Distribution of data events in the tracker as a function of reconstructed neutrino energy with statistical errors.

of 3.88×10^{29} scattering centers in the ECAL, with 47% being scintillator and 53% being lead.

II..6 Calculating a Cross Section

To calculate a cross section, we took the distribution of events in data, shown as a function of neutrino energy in FIG. 21 and 22 for tracker and ECAL events, respectively, and subtracted the estimated background, normalized by the relative number of data and Monte Carlo events as described above. This gives us the background-subtracted distributions shown in FIG. 23 and 24. We then applied the unfolding to obtain our distributions as functions of true variables, seen in FIG. 25 and 26. We next divided by our efficiency resulting in the distributions shown as FIG. 27 and 28.

We divided the ECAL distribution by the number of ECAL scattering centers and the tracker distribution by the number of tracker scattering to get cross sections in the tracker and ECAL, multiplied by the integrated flux. To extract the lead-to-scintillator cross section ratio from these dstributions, we realized that the cross section of a typical nucleon in the ECAL is the average of the scintillator and lead cross sections, weighted according to their relative abundances in the ECAL. Then, $\sigma_{ECAL} = f_{Pb}\sigma_{Pb} + f_{CH}\sigma_{CH}$, implying that $\sigma_{Pb} = \sigma_{ECAL}/f_{Pb} - \sigma_{CH}f_{CH}/f_{Pb}$,

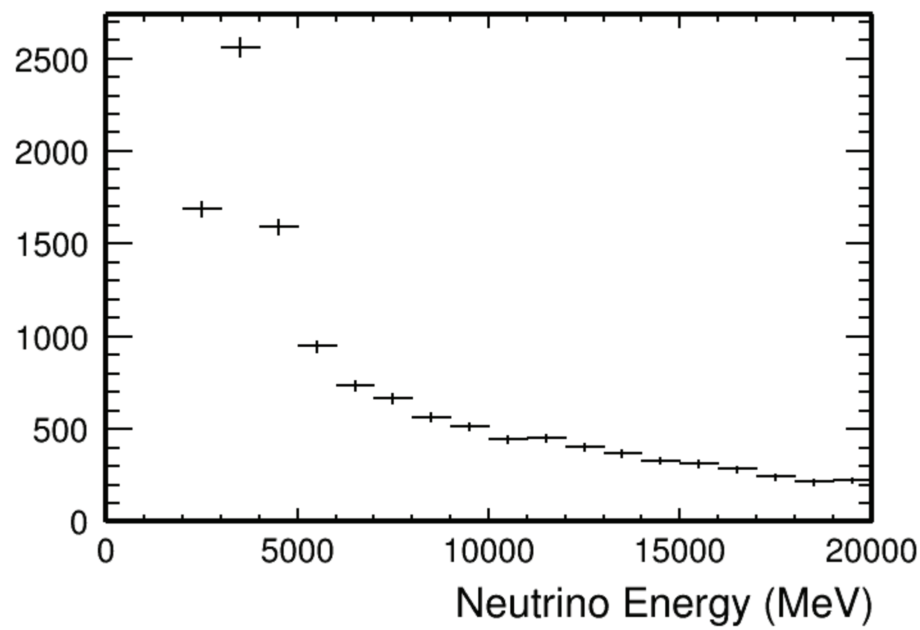

FIG. 22. Distribution of data events in the ECAL as a function of reconstructed neutrino energy with statistical errors.

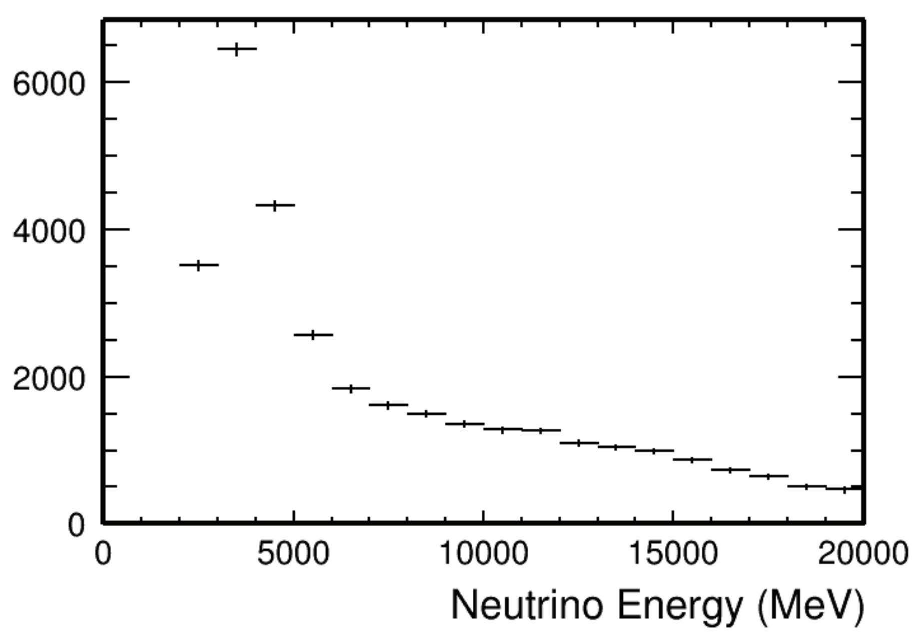

FIG. 23. Background subtracted distribution of events in the tracker data as a function of reconstructed energy with statistical and systematic errors.

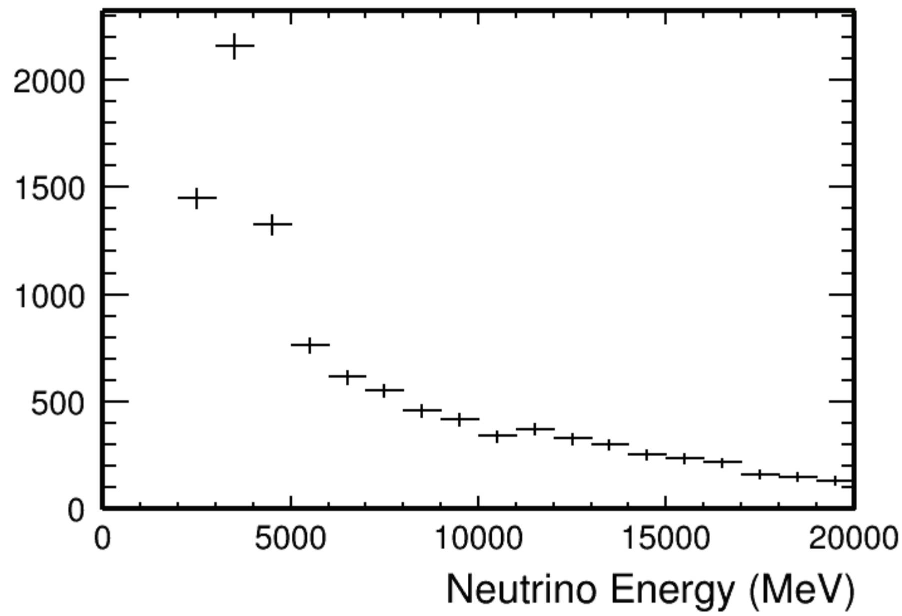

FIG. 24. Background subtracted distribution of events in the ECAL data as a function of reconstructed energy with statistical and systematic errors.

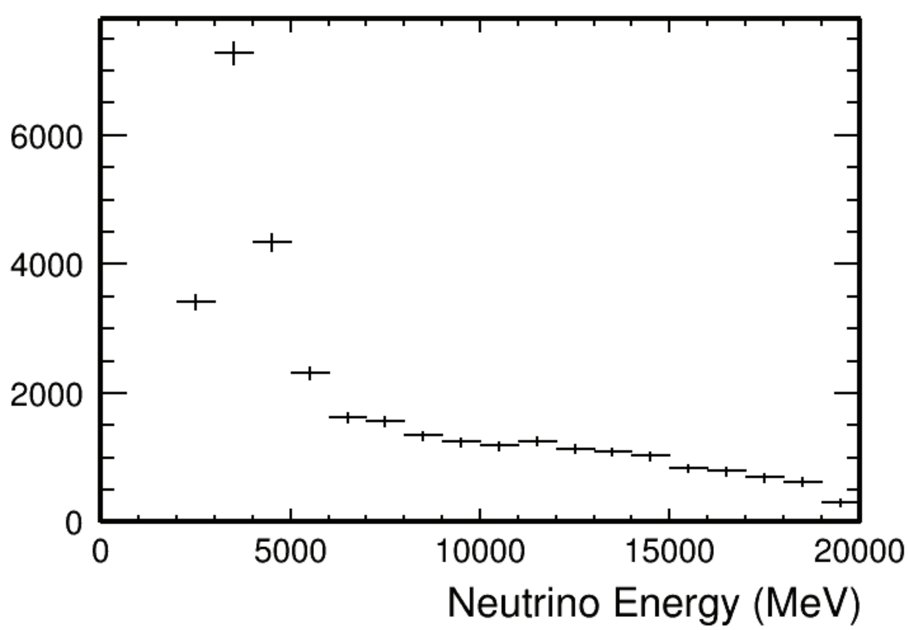

FIG. 25. Unfolded distribution of events in the tracker data as a function of unfolded neutrino energy with statistical and systematic errors.

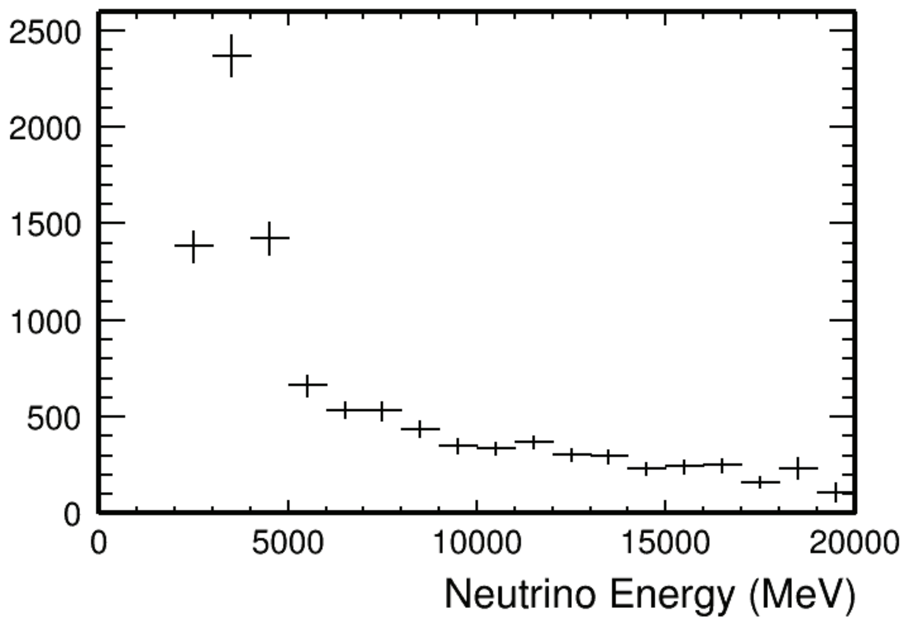

FIG. 26. Unfolded distribution of events in the ECAL data as a function of unfolded neutrino energy with statistical and systematic errors.

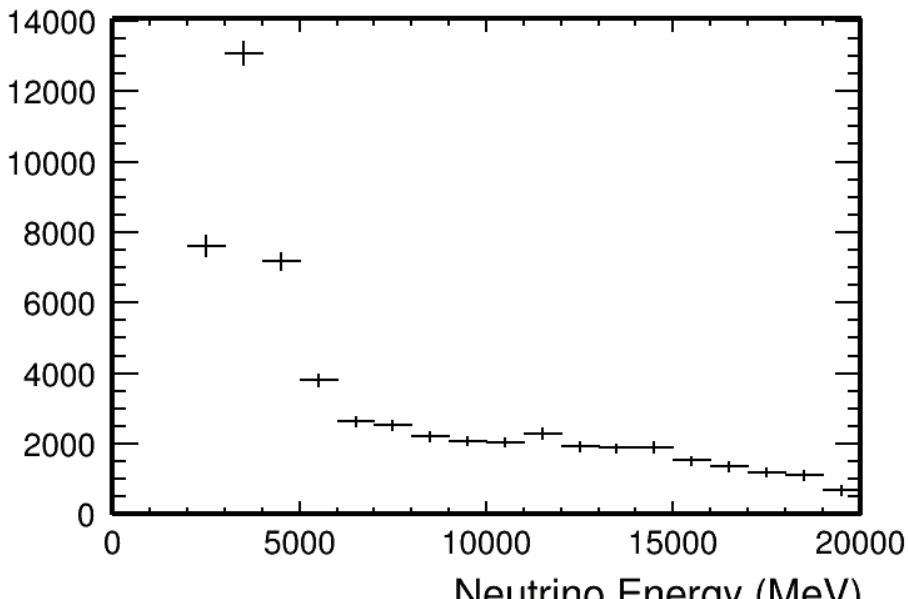

FIG. 27. Efficiency-corrected distribution of events in the tracker data as a function of unfolded neutrino energy with statistical and systematic errors.

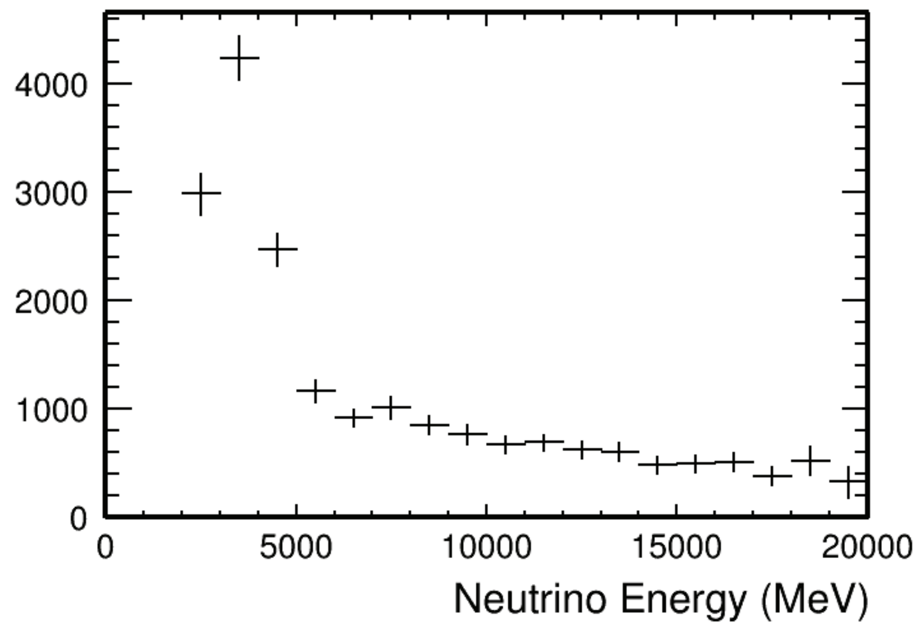

FIG. 28. Efficiency-corrected distribution of events in the ECAL data as a function of unfolded neutrino energy with statistical and systematic errors.

where σ_{ECAL} is the cross section of an average particle in the ECAL, σ_{Pb} and σ_{CH} refer to the cross sections of the lead and scintillator individually, and f_{Pb} and f_{CH} are the fraction of the ECAL which is lead or scintillator, respectively. Since σ_{CH} is the same as the cross section in the tracker, $\sigma_{Pb}/\sigma_{CH} = (\sigma_{ECAL}/f_{Pb} - \sigma_{CH} f_{CH}/f_{Pb})/\sigma_{CH}$ may be directly computed from the obtained distributions.

After having applied this analysis, we obtained the cross section ratio distributions as functions of energy and Bjorken x. The overlayed data and Monte Carlo plots for these distributions in unfolded variables are shown in FIG. 29 and 30. The ratio of the data to Monte Carlo distributions are shown as FIG. 31 and 32. We see that, as a function of energy, the data distribution matches the Monte Carlo relatively closely, although at low energy, there is a 1.7 σ excess in the data over the Monte Carlo. For the distributions as a function of Bjorken x, we see that there is a very significant deficit in data relative to Monte Carlo at low Bjorken x, and a slight excess at high values. These distributions may be compared to those obtained by the Tice analysis[1] in the upstream targets, as seen in FIG. 33 and 34. We note that he had also observed the data deficit at low values of Bjorken x and the excess at high values, although the deficit was not as pronounced, perhaps due to differences in binning. Plots of the cross section ratio functions of muon angle, muon energy, nuclear recoil energy, and inelasticity are shown in the Appendix.

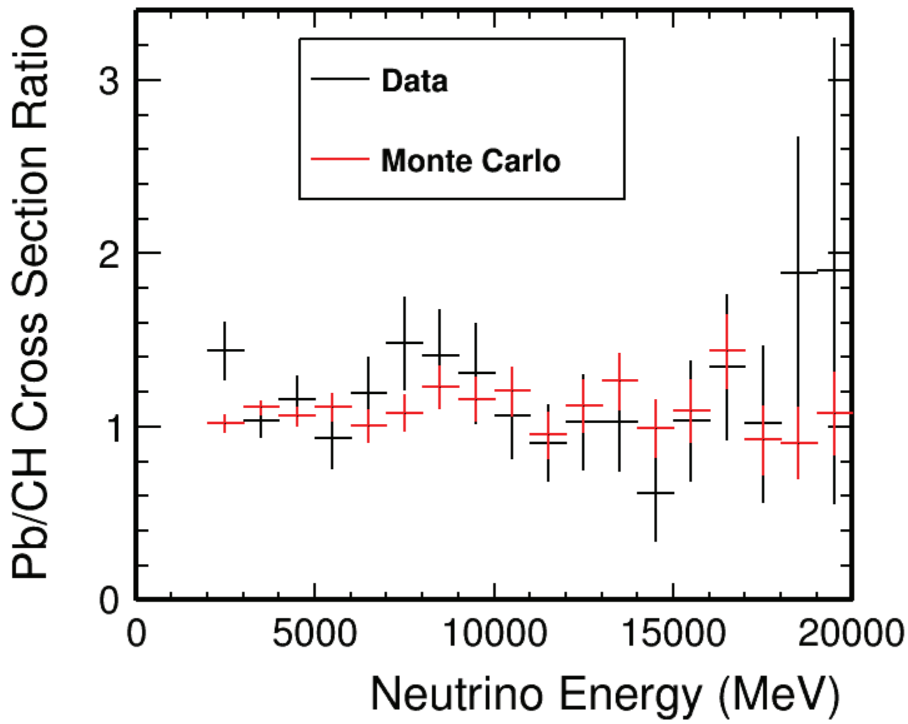

FIG. 29. Cross section ratio between lead and scintillator in the data and Monte Carlo as a function of unfolded neutrino energy.

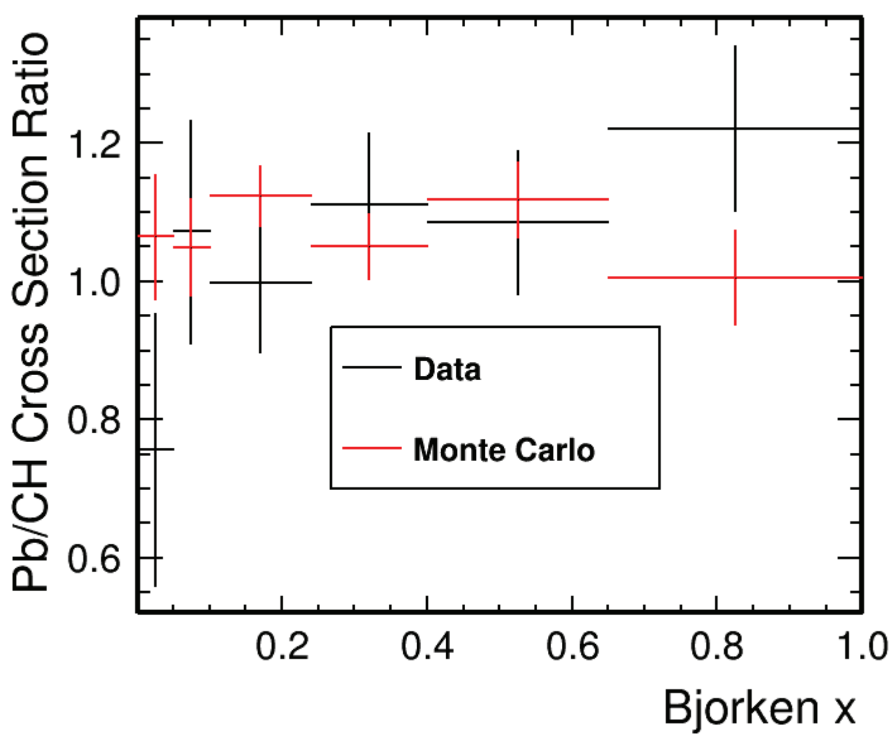

FIG. 30. Cross section ratio between lead and scintillator in the data and Monte Carlo as a function of unfolded Bjorken x.

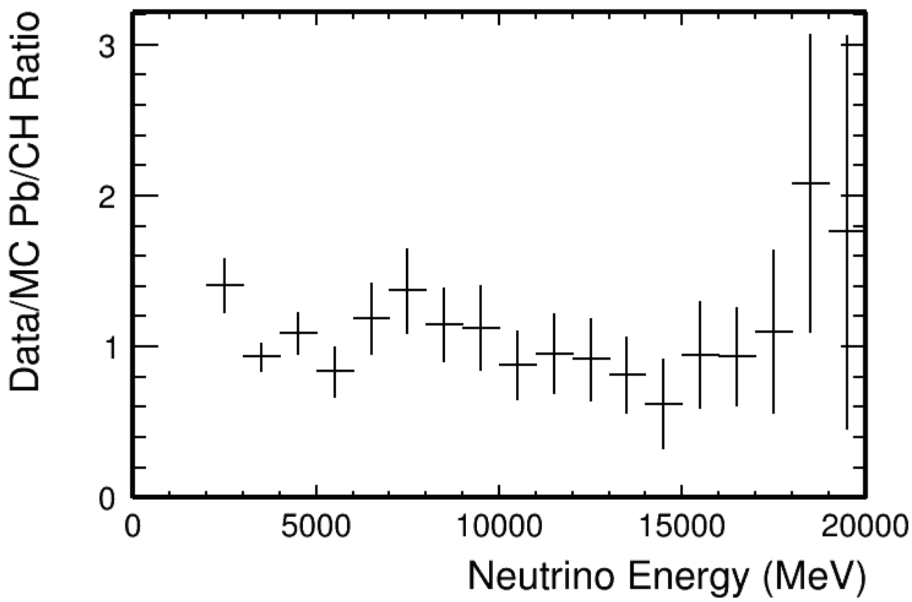

FIG. 31. Ratio of data to Monte Carlo $\sigma Pb/\sigma CH$ as a function of unfolded neutrino energy.

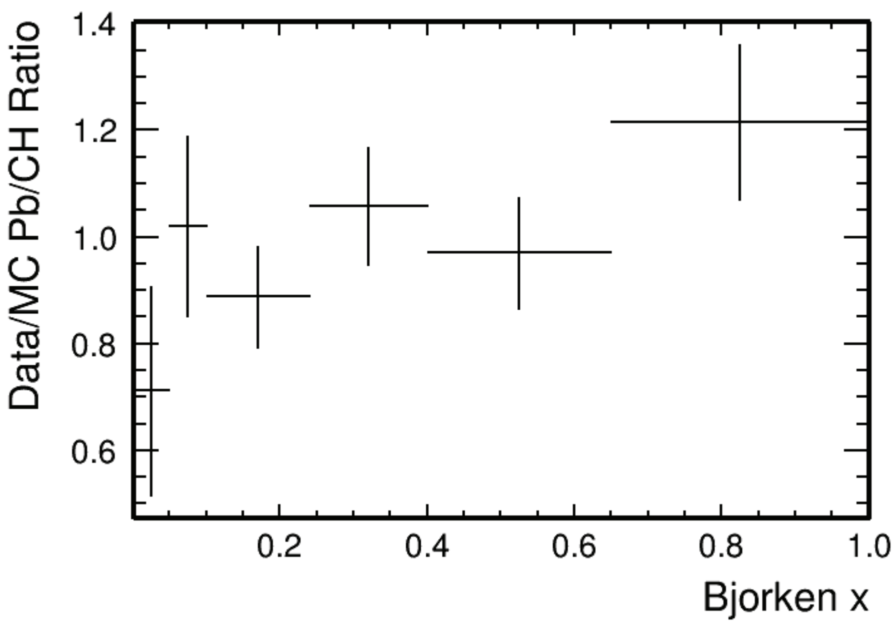

FIG. 32. Ratio of data to Monte Carlo $\sigma Pb/\sigma CH$ as a function of unfolded Bjorken x.

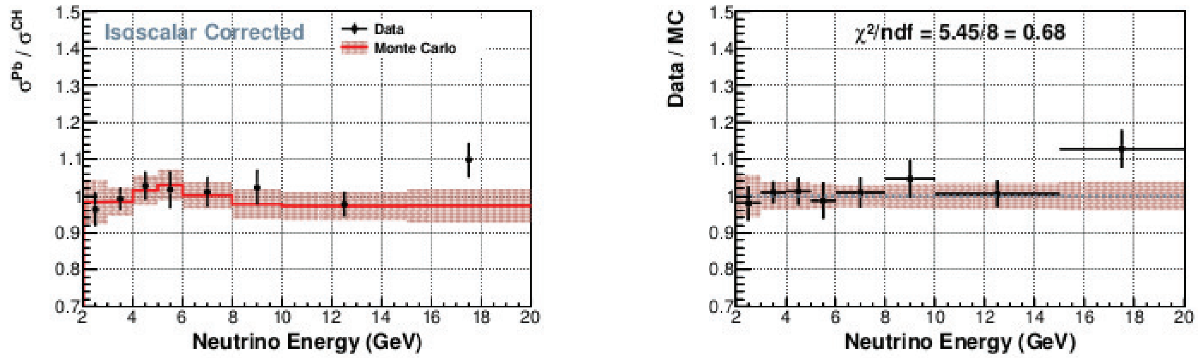

(e) Lead

(f) Data to Monte Carlo ratio for lead

FIG. 33. Findings from the Tice analysis for the data and Monte Carlo cross section ratios, as well as the ratio of data to Monte Carlo as a function of energy. (Fig. 6.1 in Brian Tice's thesis.[1])

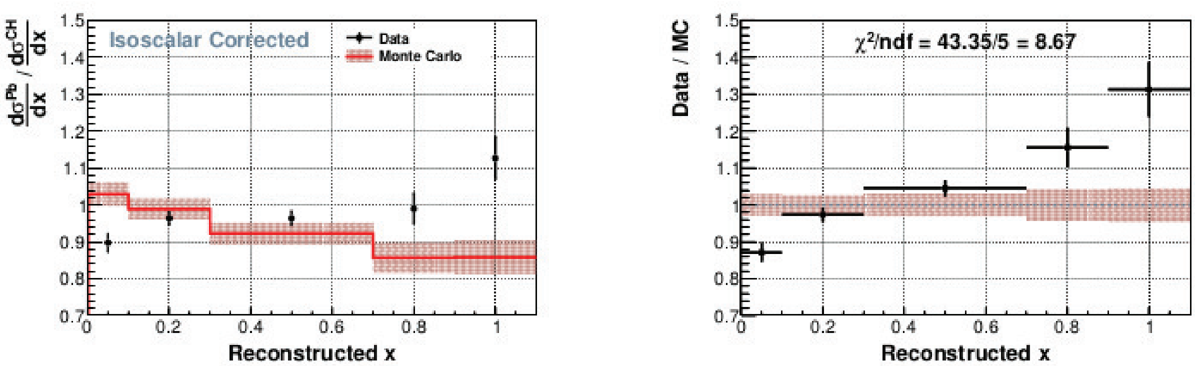

(e) Lead

(f) Data to Monte Carlo ratio for lead

FIG. 34. Findings from the Tice analysis for the data and Monte Carlo cross section ratios, as well as the ratio of data to Monte Carlo as a function of Bjorken x. (Fig. 6.2 in Brian Tice's thesis.[1])

II..7 Errors

There were two types of errors considered in this analysis: statistical errors and systematic errors. The statistical errors were calculated in the usual manner as the square root of the number of data entries in a given bin and the usual error propagation. The propagation through the unfolding was taken care of automatically by MnvUnfold. To calculate the systematic errors in the Monte Carlo, we used the many universes method.[6] To do this, we varied different paramters used to produce the Monte Carlo within their uncertainties, with each variation being a separate "universe." The analysis was repeated in each of these universes. In each histogram bin, we took the RMS of the value across all the universes as the systematic error in that bin. We considered both vertical and lateral systematic errors. The lateral errors represent uncertainties in measurements of certain quantities shifting events between bins of the histogram, while the vertical errors would have the result of changing the overall number of events. We considered four sources of vertical systematic errors: the beam focus, which represented the uncertainty in how our pion beam is focused; the NA49 error, which tells us our uncertainty in the pion production in regions covered by the NA49 experiment at CERN; the tertiary error, which tells us the uncertainty in the neutrino production due to particle decays not covered by NA49; and the GENIE error, which tells us errors in how GENIE models the neutrino cross section and interactions in the final state.[7] The relative importances of these, plus the Monte Carlo statistical error, are shown in FIG. 35 and 36. We considered two sources for the lateral systematic errors: uncertainty in the muon energy and uncertainty in the nuclear recoil energy. We see that, in our cross section ratios, the Monte Carlo statistical errors dwarf the systematic errors.

III. Conclusion

We have obtained cross section ratios between lead and scintillator as functions of different variables. We see that the cross section ratios look similar for Monte Carlo and data as a function of energy, although there is a data excess at low energy. When plotted as functions of Bjorken x, the data show a significant deficit at low values, and a less significant excess at high values. This is similar to what was observed the upstream nuclear targets of the MINERvA detector in the Tice analysis. Therefore, GENIE does not properly model neutrino cross sections in different nuclei.

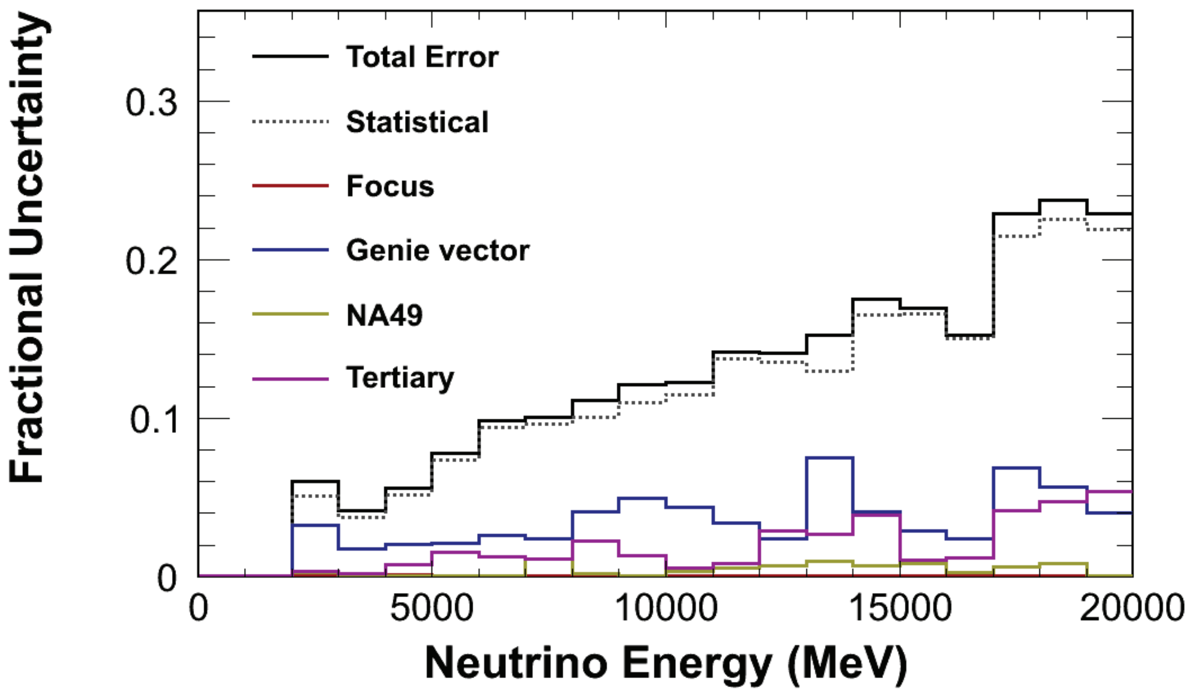

FIG. 35. The contributions of various errors to the total error in the Monte Carlo lead-scintillator ratio. This is shown as a function of true neutrino energy.

IV. Future Work

In the future, it would be useful to apply an isoscalar correction to the results, which would correct for the differences in the number of neutrons and protons in the different regions of the detector. Also, we would like to isolate just the DIS sample and see if there is any change.

V. Acknowledgements

I would like to thank Professor Nelson and Josh Devan for introducing me to this project, teaching me the analysis tools, and otherwise providing invaluable help. I would also like to thank the MINERvA collaboration for providing the analysis software and data.

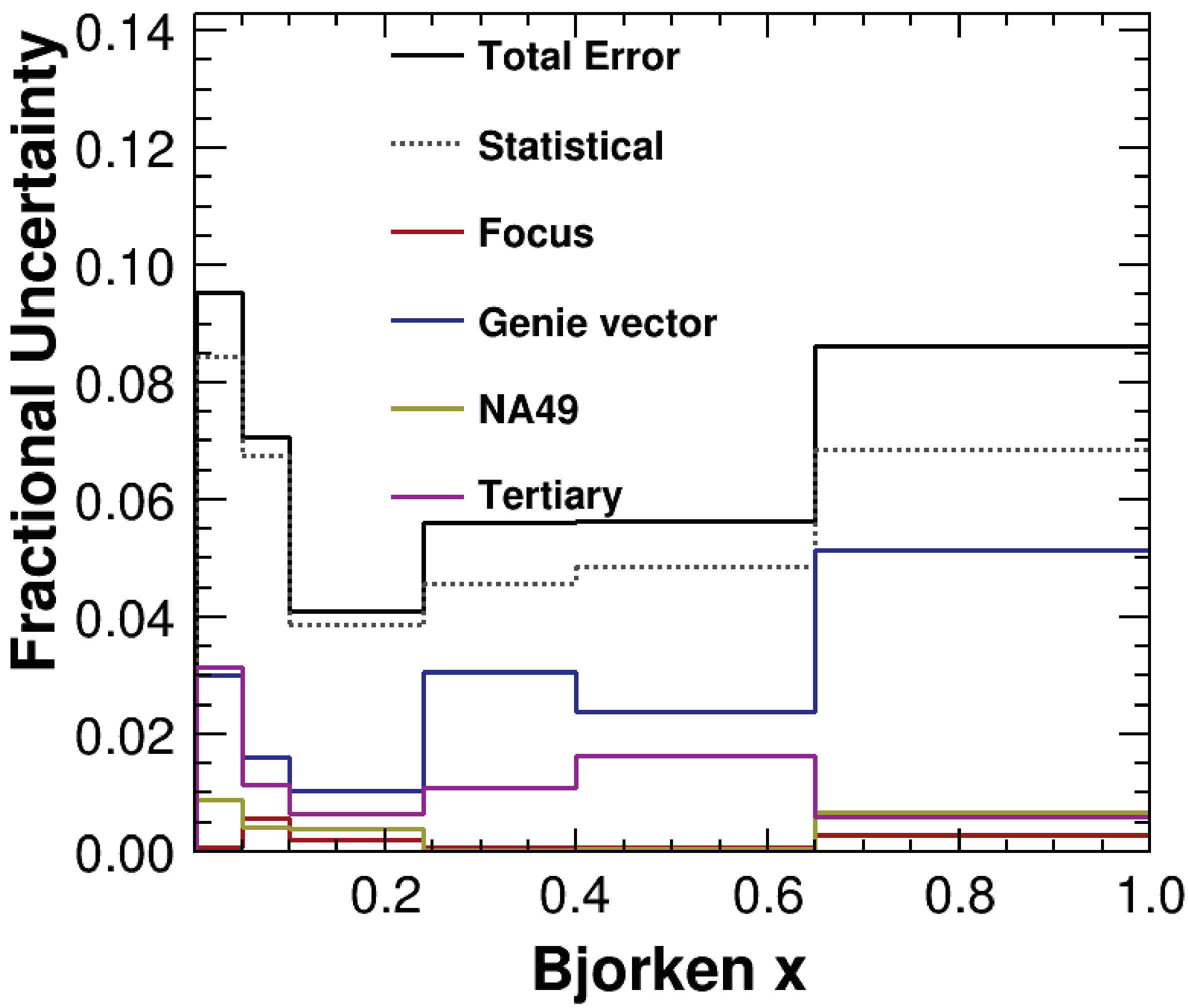

FIG. 36. The contributions of various errors to the total error in the Monte Carlo lead-scintillator ratio. This is shown as a function of true Bjorken x.

VI. Appendix A: Efficiencies

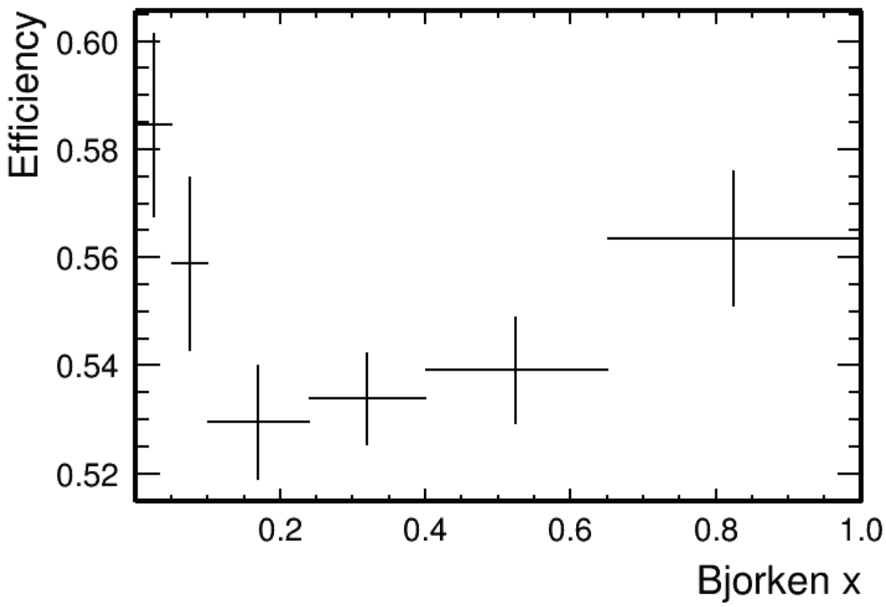

FIG. 37. Efficiency as a function of true Bjorken x in the tracker Monte Carlo with statistical and systematic errors.

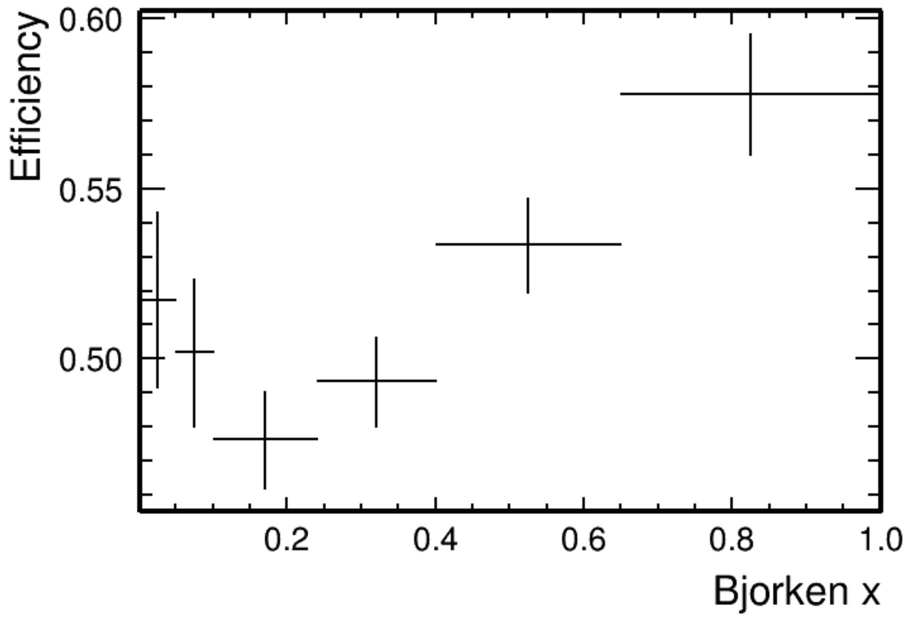

FIG. 38. Efficiency as a function of true Bjorken x in the ECAL Monte Carlo with statistical and systematic errors.

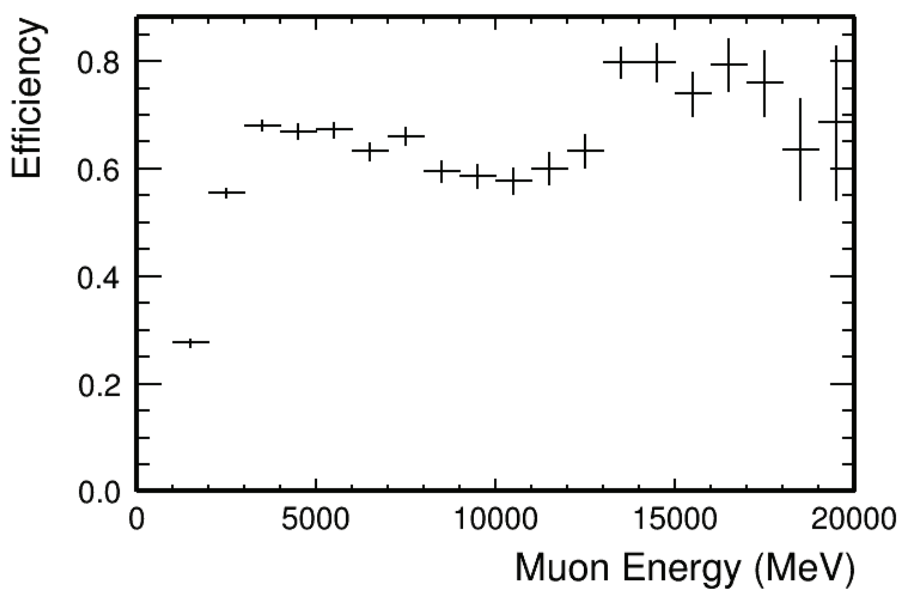

FIG. 39. Efficiency as a function of true muon energy in the tracker Monte Carlo with statistical and systematic errors.

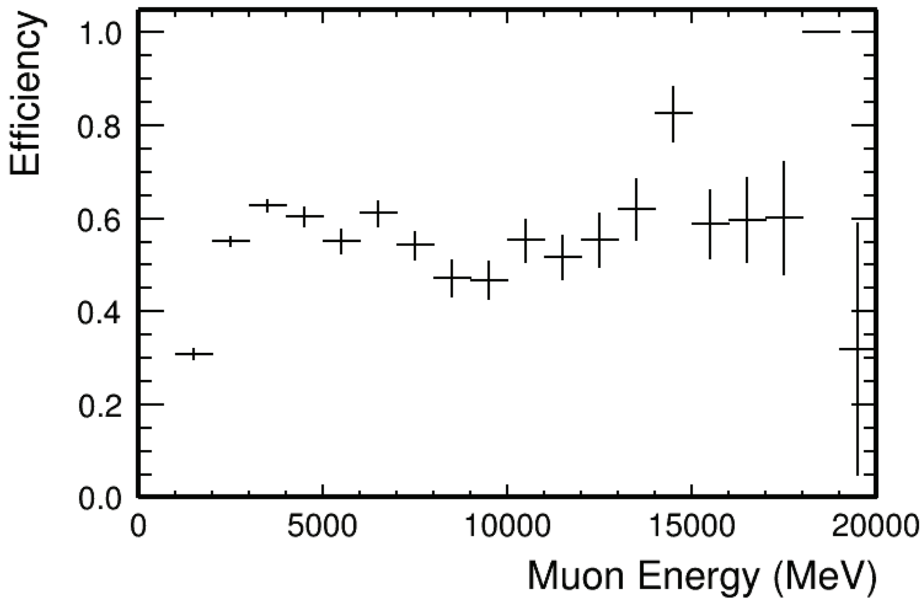

FIG. 40. Efficiency as a function of true muon energy in the ECAL Monte Carlo with statistical and systematic errors.

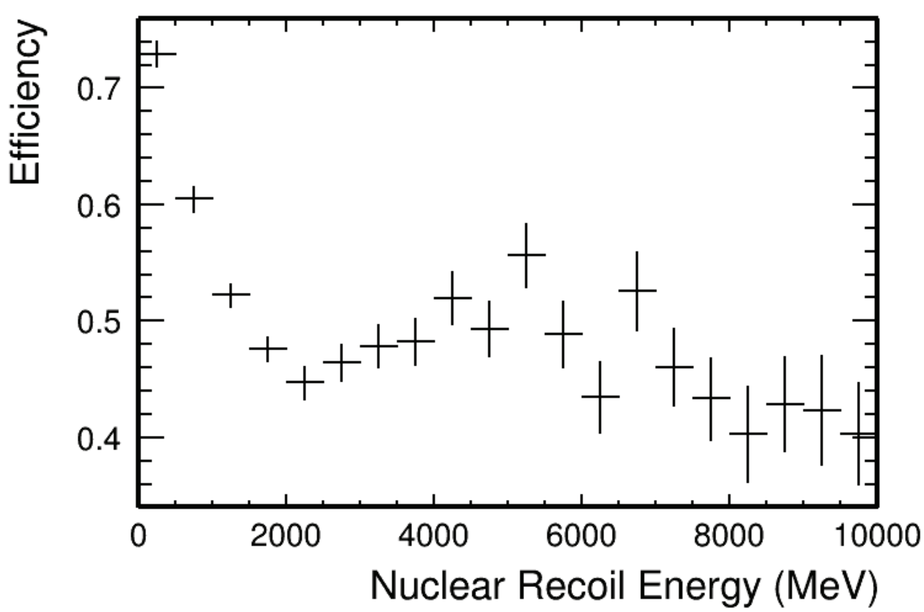

FIG. 41. Efficiency as a function of true nuclear recoil energy in the tracker Monte Carlo with statistical and systematic errors.

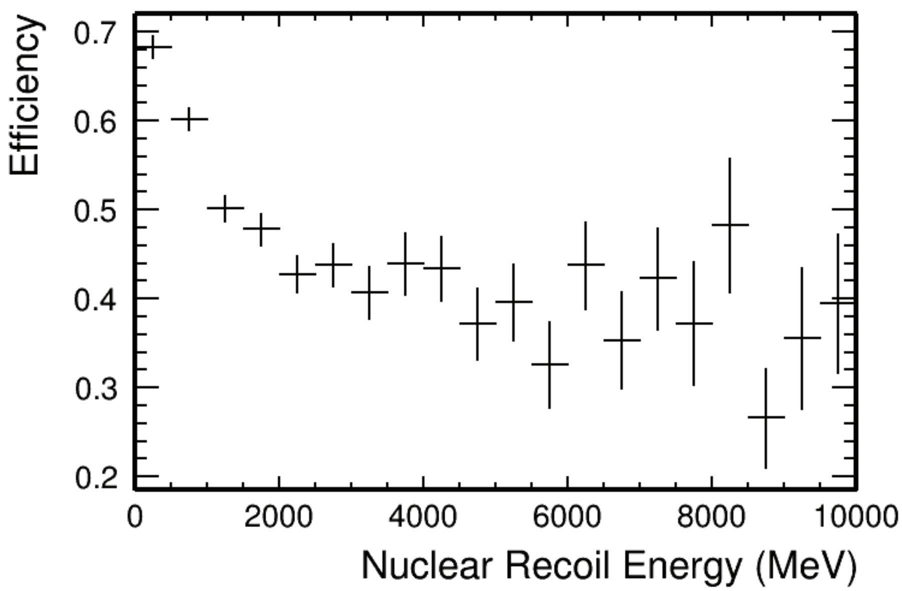

FIG. 42. Efficiency as a function of true nuclear recoil energy in the ECAL Monte Carlo with statistical and systematic errors.

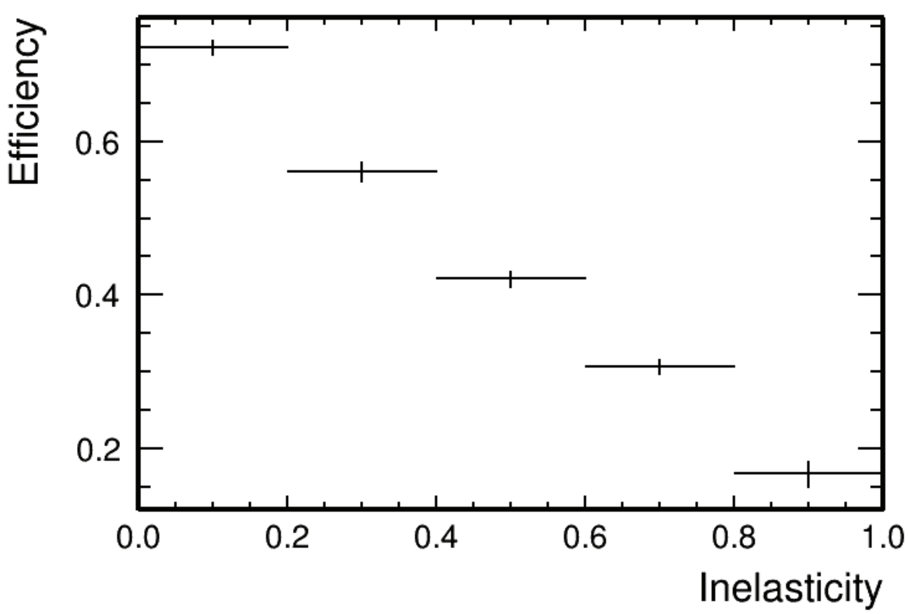

FIG. 43. Efficiency as a function of true inelasticity in the tracker Monte Carlo with statistical and systematic errors.

VII. Appendix B: Backgrounds

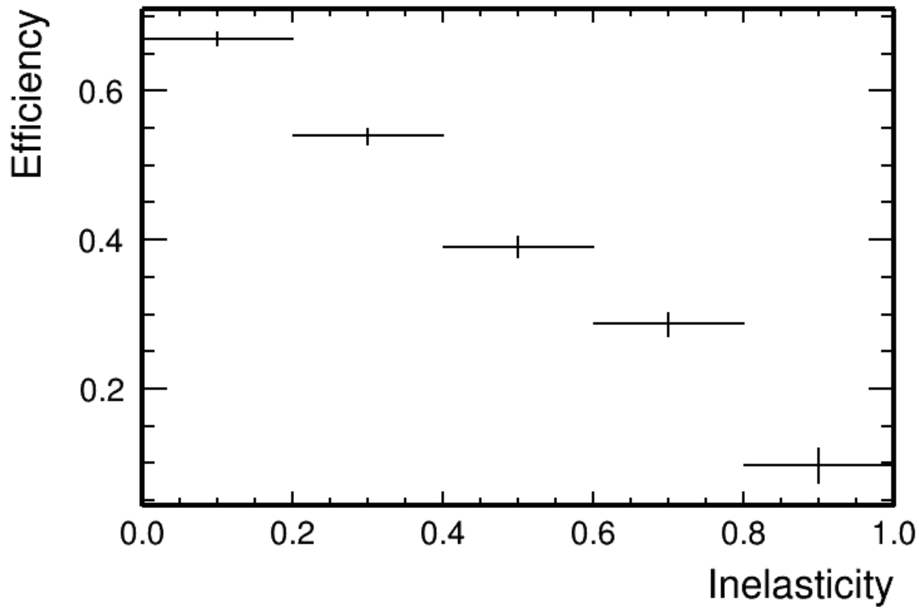

FIG. 44. Efficiency as a function of true inelasticity in the ECAL Monte Carlo with statistical and systematic errors.

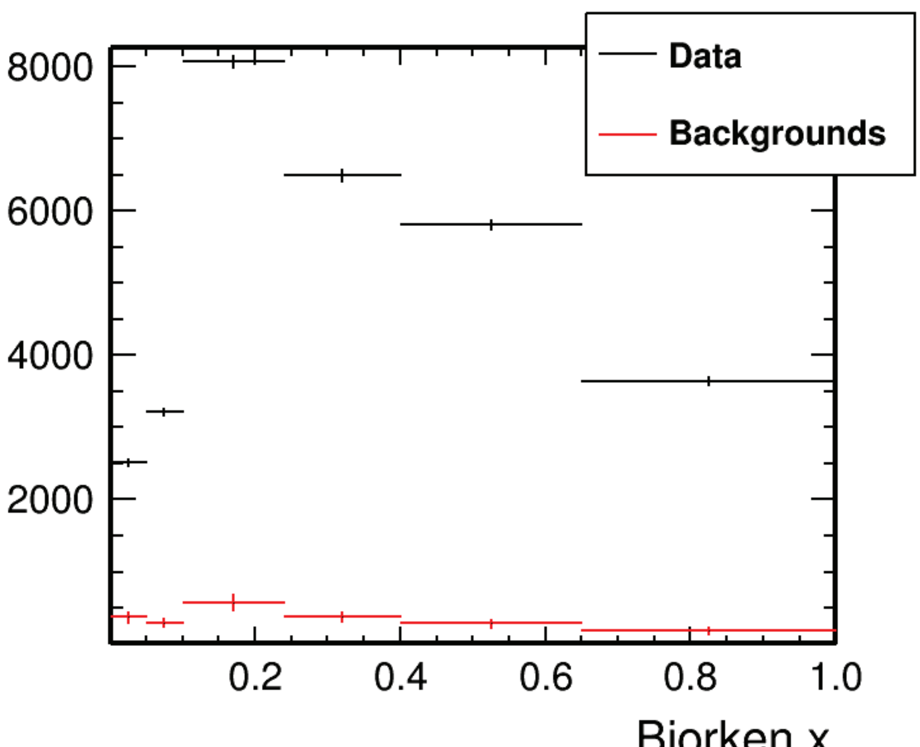

FIG. 45. Backgrounds estimated from Monte Carlo and data distributions as a function of reconstructed Bjorken x in the tracker. The background has statistical and systematic errors, while the data have just statistical errors.

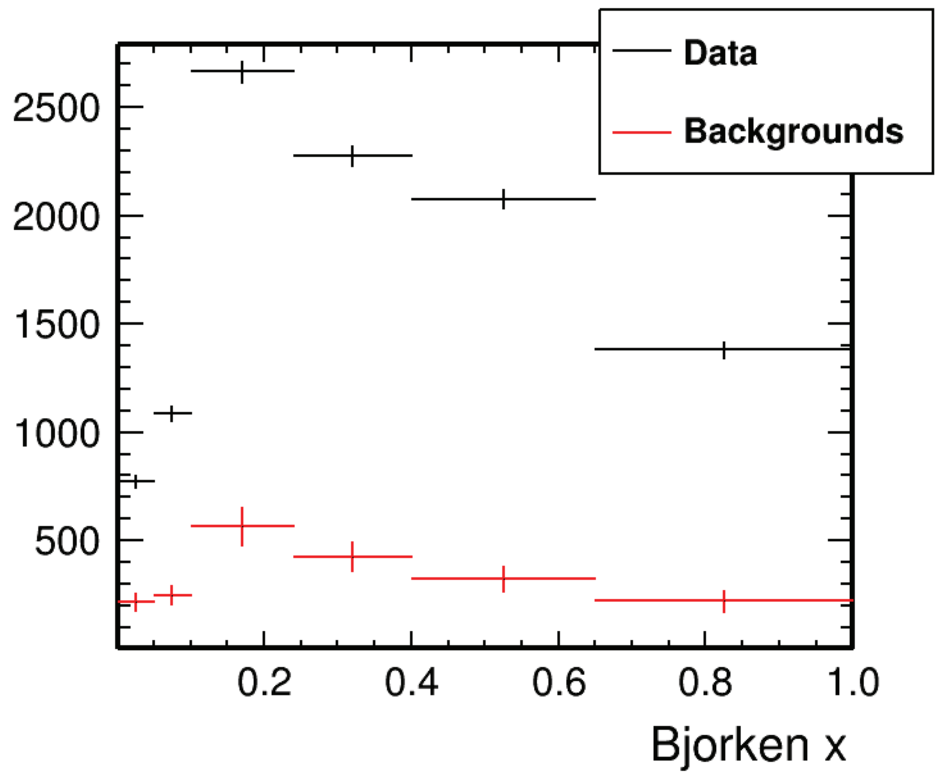

FIG. 46. Backgrounds and data distributions as a function of reconstructed Bjorken x in the ECAL. The background has statistical and systematic errors, while the data have just statistical errors.

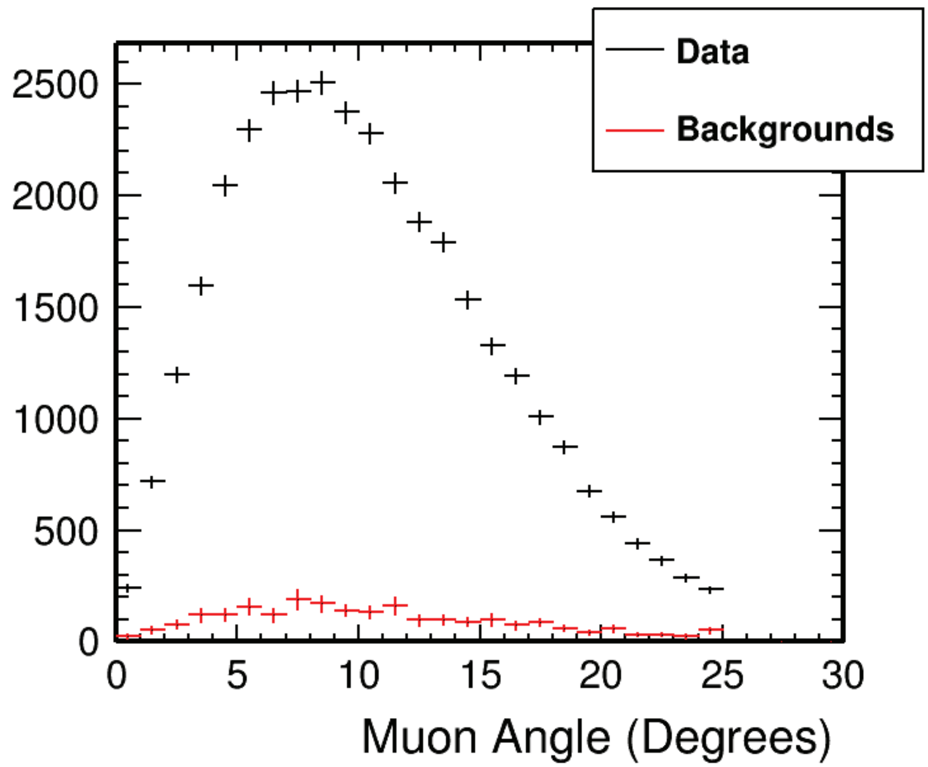

FIG. 47. Backgrounds and data distributions as a function of reconstructed muon angle in the tracker. The background has statistical and systematic errors, while the data have just statistical errors.

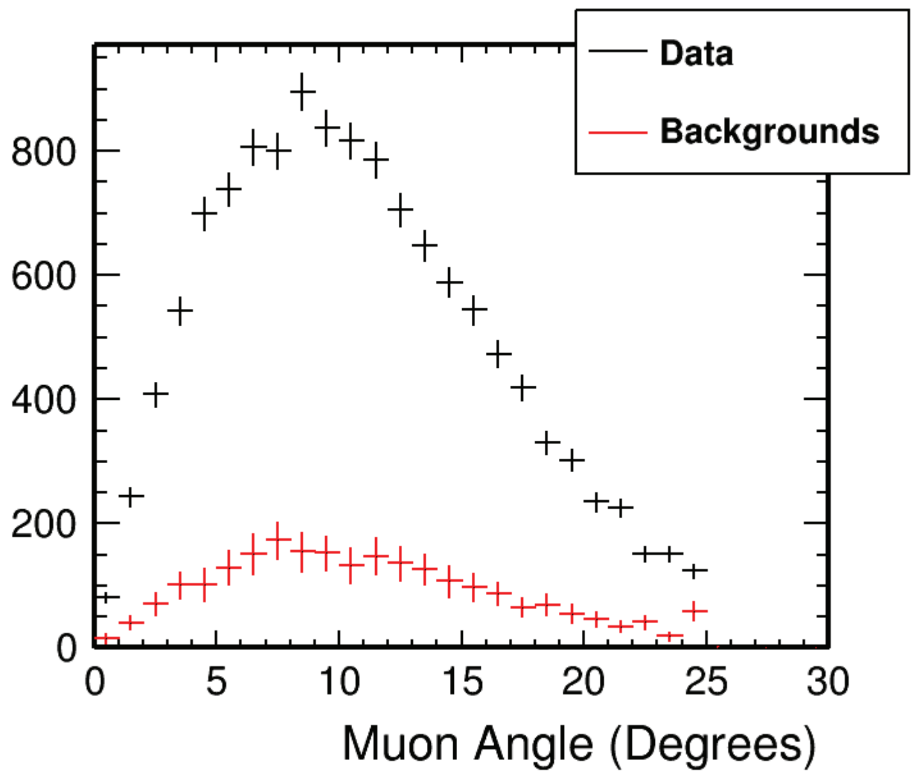

FIG. 48. Backgrounds and data distributions as a function of reconstructed muon angle in the ECAL. The background has statistical and systematic errors, while the data have just statistical errors.

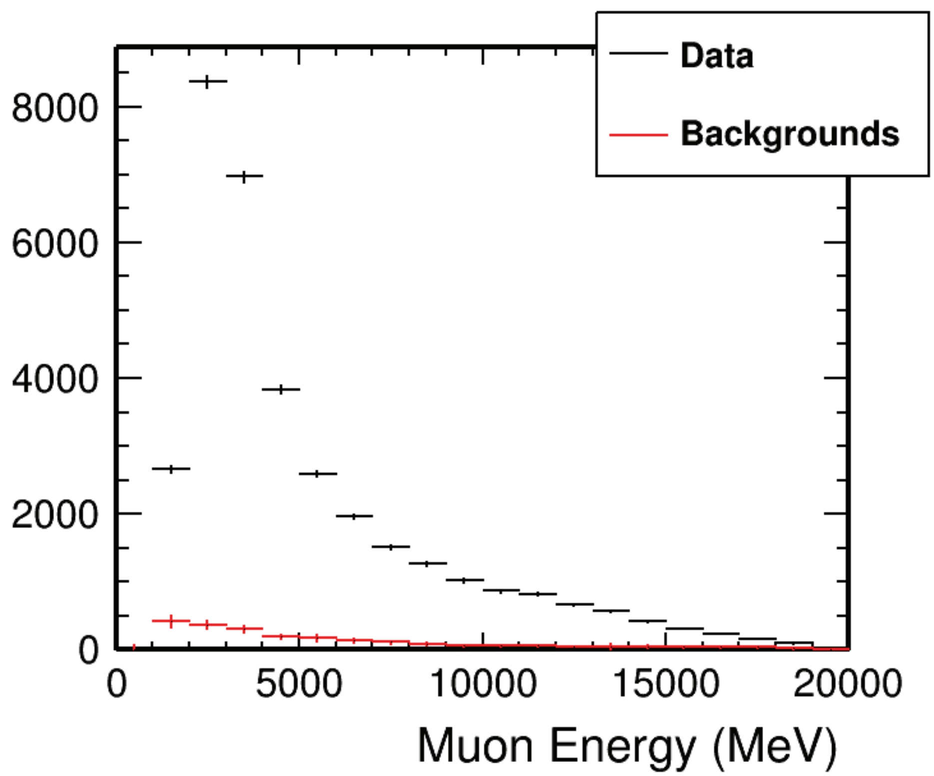

FIG. 49. Backgrounds and data distributions as a function of reconstructed muon energy in the tracker. The background has statistical and systematic errors, while the data have just statistical errors.

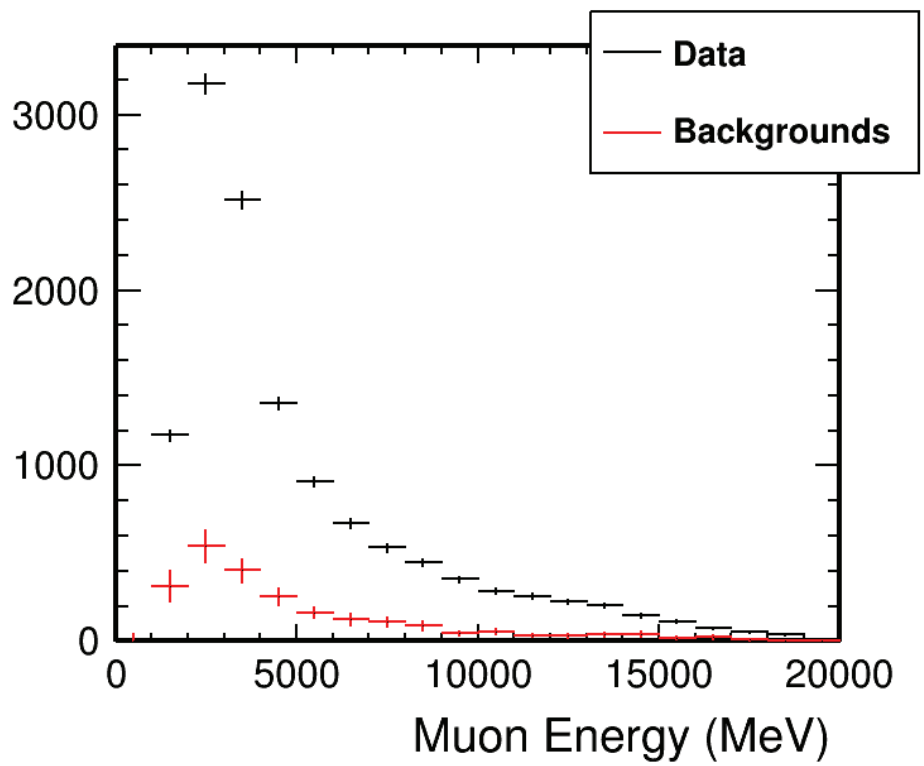

FIG. 50. Backgrounds and data distributions as a function of reconstructed muon energy in the ECAL. The background has statistical and systematic errors, while the data have just statistical errors.

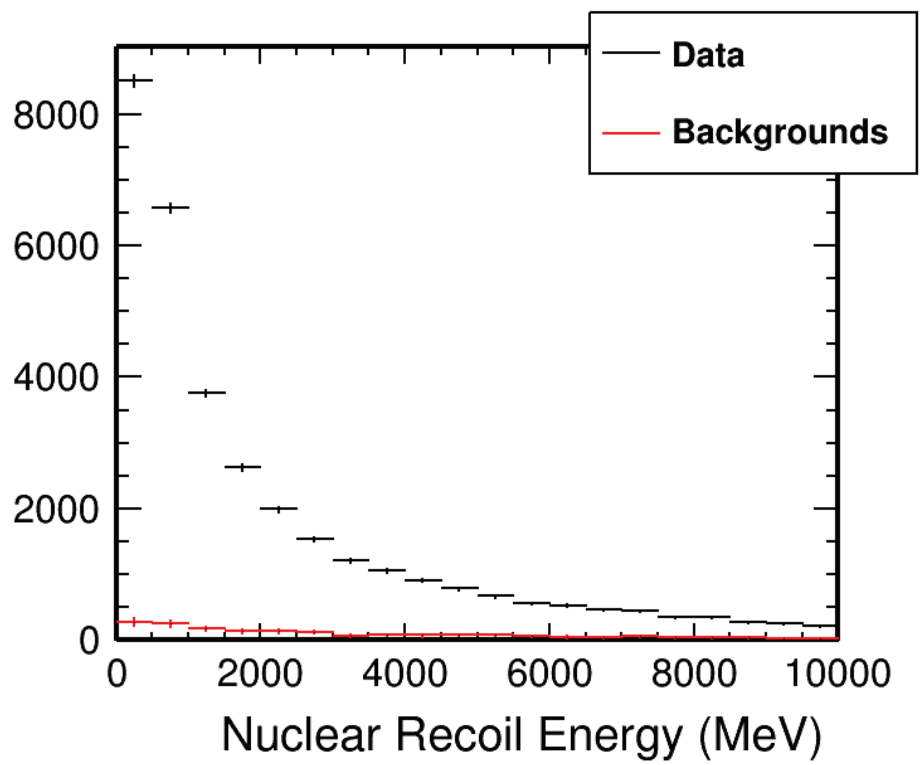

FIG. 51. Backgrounds and data distributions as a function of reconstructed nuclear recoil energy in the tracker. The background has statistical and systematic errors, while the data have just statistical errors.

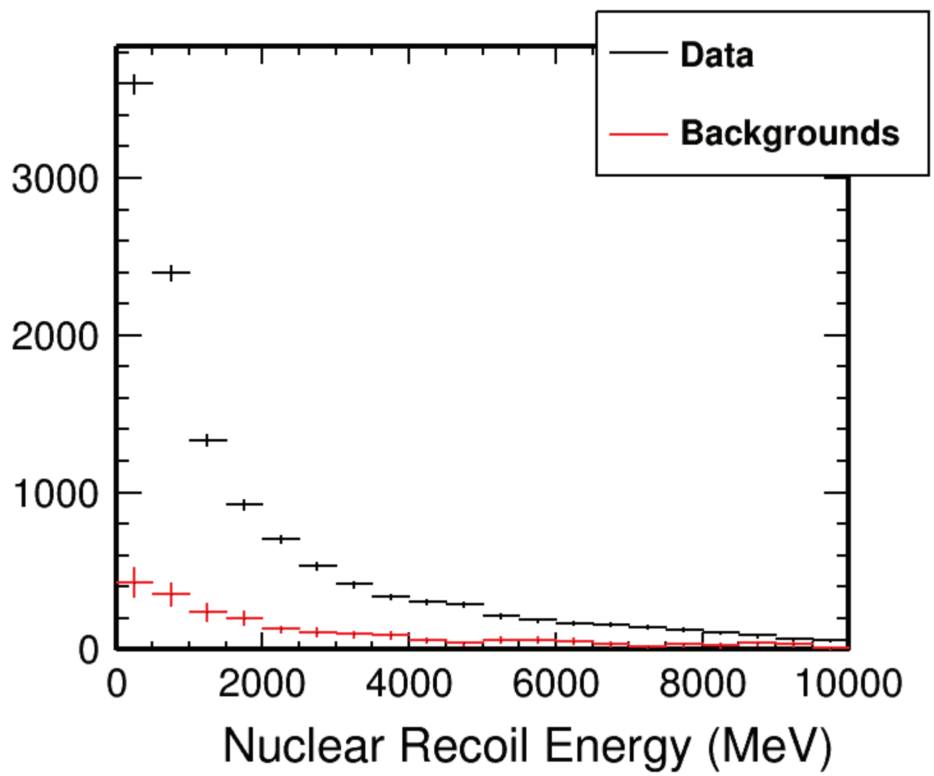

FIG. 52. Backgrounds and data distributions as a function of reconstructed nuclear recoil energy in the ECAL. The background has statistical and systematic errors, while the data have just statistical errors.

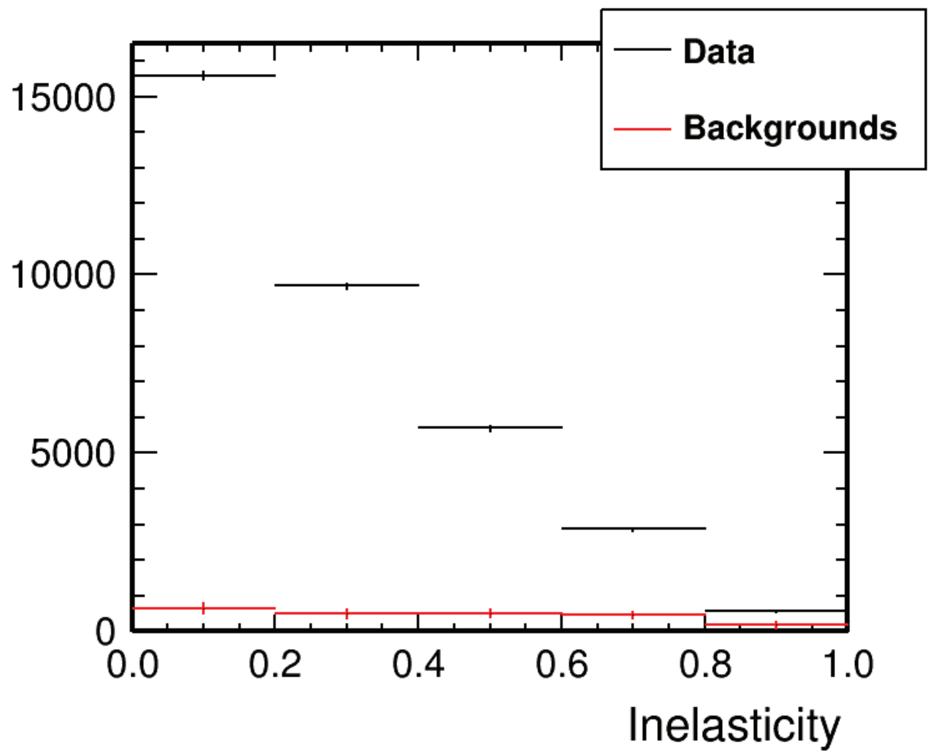

FIG. 53. Backgrounds and data distributions as a function of reconstructed inelasticity in the tracker. The background has statistical and systematic errors, while the data have just statistical errors.

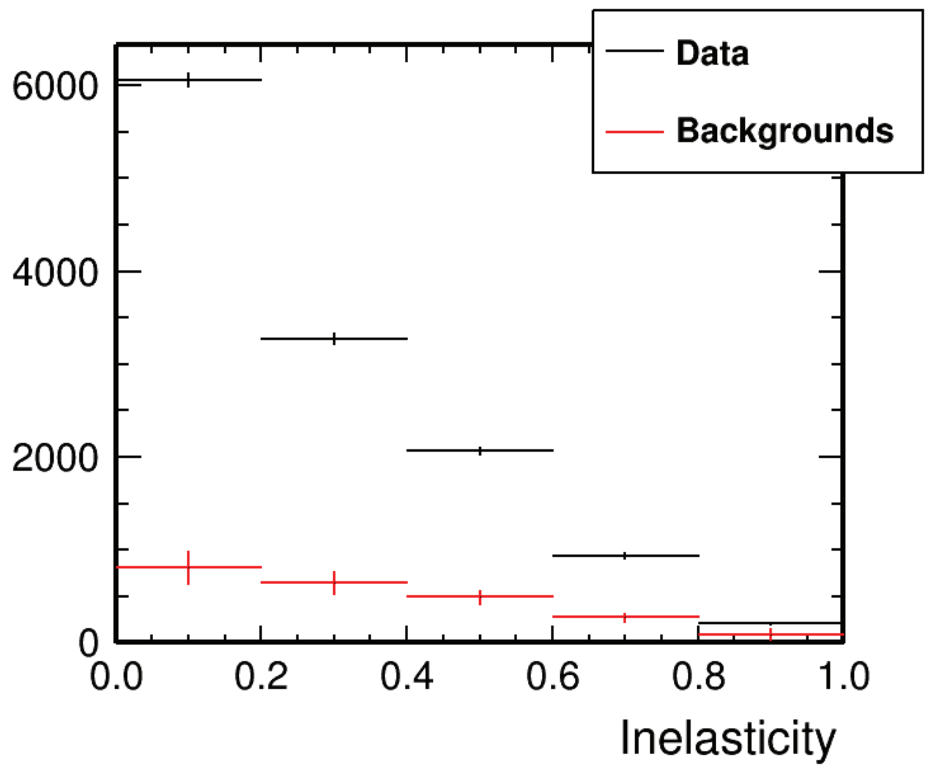

FIG. 54. Backgrounds and data distributions as a function of reconstructed inelasticity in the ECAL. The background has statistical and systematic errors, while the data have just statistical errors.

VIII. Appendix C: Cross Section Ratios

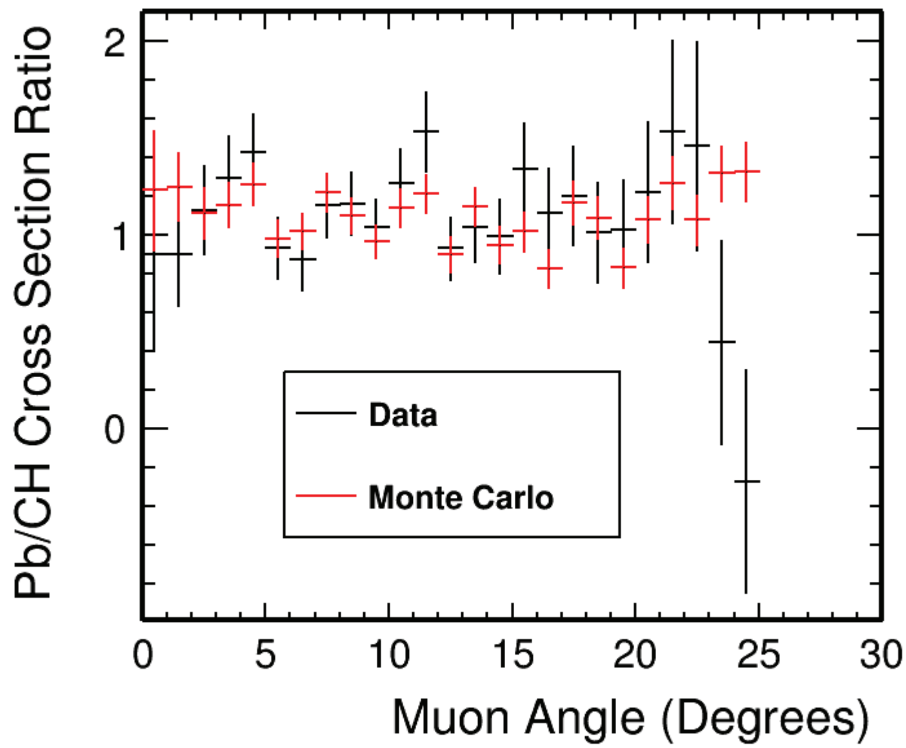

FIG. 55. Cross section ratio between lead and scintillator in the data and Monte Carlo as a function of true muon angle. The Monte Carlo and data have statistical and systematic errors.

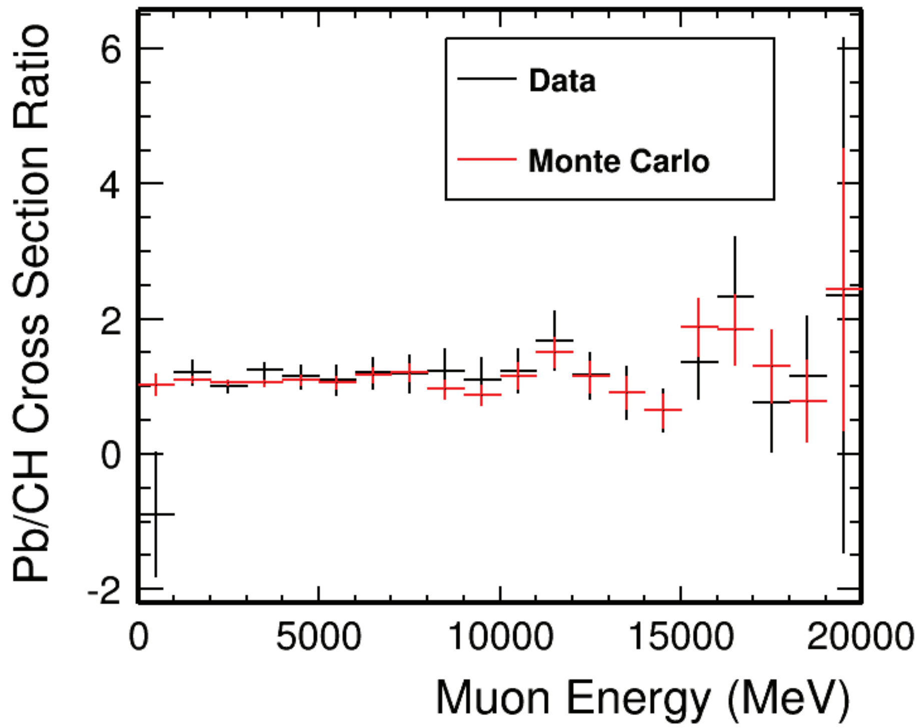

FIG. 56. Cross section ratio between lead and scintillator in the data and Monte Carlo as a function of true muon energy. The Monte Carlo and data have statistical and systematic errors.

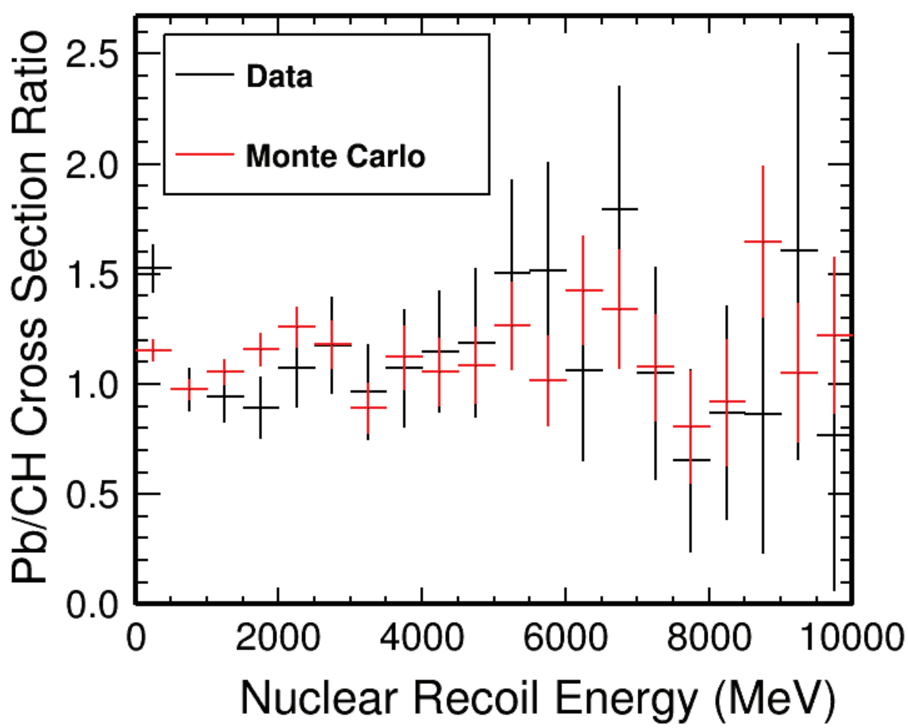

FIG. 57. Cross section ratio between lead and scintillator in the data and Monte Carlo as a function of true nuclear recoil energy. The Monte Carlo and data have statistical and systematic errors.

References

[1] Tice, B.G. "Measurement of Nuclear Dependence in Inclusive Charged Current Neutrino Scattering." Dissertation for Rutgers, the State University of New Jersey. January 2014. Retreived from MINERvA docdb, http://minerva-docdb.fnal.gov:8080/cgi-bin/ShowDocument?docid=9464, on November 5, 2014.

[2] Tice, B.G. et al. (MINERvA Collaboration). Measurement of Ratios of Charged-Current Cross Sections on C, Fe, and Pb to CH at Neutrino Energies 2-20 GeV. Physical Review Letters. Volume 12, Issue 23, Article Number 231801. June 9, 2014. Retrieved from Physical Review Letters, http://journals.aps.org/prl/abstract/10.1103/PhysRevLett.112.231801, on September 14, 2014.

[3] Acciarri, R. et al. (ArgoNeut Collaboration). Measurements of inclusive muon neutrino and antineutrino charged current differential cross sections on argon in the NuMI antineutrino beam. Physical Review D. Volume 89, Issue 11, Article Number 112003. June 9, 2014. Retrieved from Physical Review D, http://journals.aps.org/prd/abstract/10.1103/PhysRevD.89.112003, on September 25, 2014.

[4] Adamson, P. et al. (MINOS Collaboration). Neutrino and antineutrino inclusive charged-current cross section measurements with the MINOS near detector. Physical Review D. Volume 81, Issue 7, Article Number 072002. April 1, 2010. Retrieved from Physical Review D, http://journals.aps.org/prd/abstract/10.1103/PhysRevD.81.072002, on September 25, 2014.

[5] Martinez, David. "First Measurement of Muon Neutrino Charged Current Quasi-elastic to Charged Current Inclusive Cross Section Ratio on a Hydrocarbon Target at Neutrino Energies 2-10 GeV." Dissertation for Centro Brasileiro de Pesquisas F sicas. August, 2014. Retreived from https://www.dropbox.com/s/y4kipdh0u7vagke/david_martinez_doctor_thesis.pdf?dl=0 on November 10, 2014.

[6] Kordosky, M. "Error bands from the many universes method." MINERvA internal document, docdb number 7433. April 4, 2012. Retrieved from

http://minerva-docdb.fnal.gov:8080/cgi-bin/ShowDocument?docid=7433 on March 29, 2015.

[7] Bravar, Alessandro. "Hadron Production Experiments." Presentation at ICFA ν panel. January 8, 2014. Retrieved from https://indico.in2p3.fr/event/8974/session/4/contribution/12/material/slides/0.pdf on April 16, 2015.

[8] Adye, Tim. "Unfolding algorithms and tests using RooUnfold." arXiv:1105.1160. May 5, 2011.

[9] D'Agostini, G. "A multidimensional unfolding method based on Bayes' theorem." Nuclear Instruments and Methods in Physics Research A 362 (1995) 487-498. Retrieved April 27, 2015.

[10] Kilmer, Jim and McFarland, Kevin. "ECAL lead sheet thickness." MINERvA internal document, docdb number 2199-v3. April 30, 2015. Retrieved from http://minerva-docdb.fnal.gov:8080/cgi-bin/ShowDocument?docid=2199 on May 1, 2015.

[11] Mousseau, Joel. "DIS Ratios Update." MINERvA internal document, docdb 10742. March 4, 2015. Retrieved from http://minerva-docdb.fnal.gov:8080/cgi-bin/ShowDocument?docid=10742 on May 11, 2015.

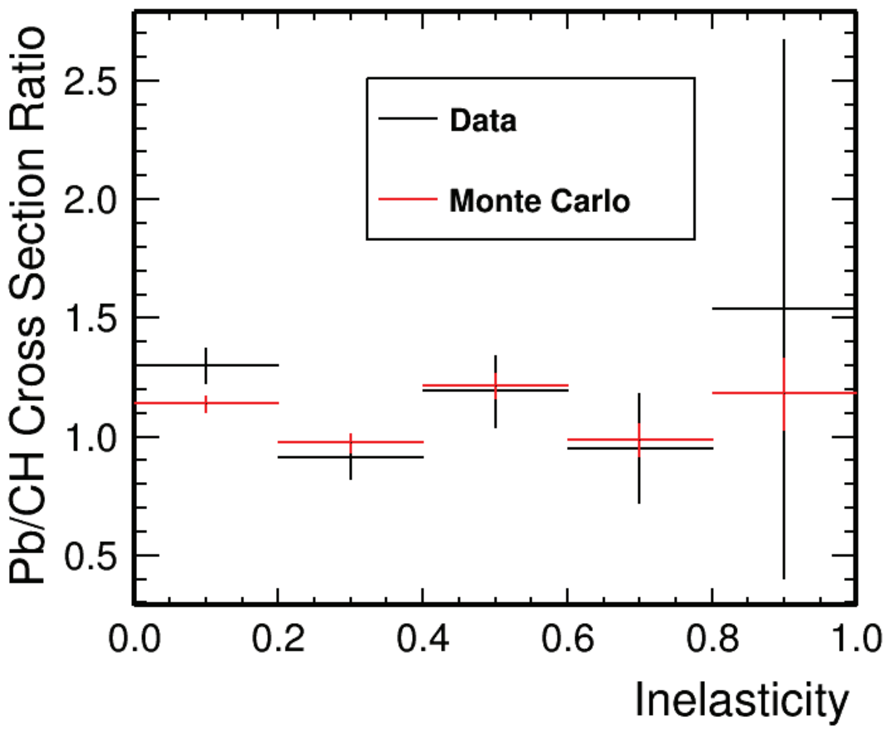

FIG. 58. Cross section ratio between lead and scintillator in the data and Monte Carlo as a function of true inelasticity. The Monte Carlo and data have statistical and systematic errors.